Acta Pharmaceutica Sinica B 2025;15(3):1589−1607

Chinese Pharmaceutical Association
Institute of Materia Medica, Chinese Academy of Medical Sciences

Acta Pharmaceutica Sinica B

www.elsevier.com/locate/apsb
www.sciencedirect.com

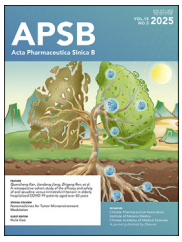

ORIGINAL ARTICLE

Parkin inhibits iron overload-induced cardiomyocyte ferroptosis by ubiquitinating ACSL4 and modulating PUFA-phospholipids metabolism

Dandan Xiao[a,b], Wenguang Chang[a], Xiang Ao[a,b], Lin Ye[a], Weiwei Wu[b], Lin Song[b], Xiaosu Yuan[a,b], Luxin Feng[c], Peiyan Wang[a,b], Yu Wang[a,b], Yi Jia[a,b], Xiaopeng Tang[b], Jianxun Wang[a,b,*]

[a]*Institute for Translational Medicine, the Affiliated Hospital of Qingdao University, Qingdao 266021, China*
[b]*School of Basic Medicine, Qingdao University, Qingdao 266071, China*
[c]*Department of Cardiovascular Medicine, the Affiliated Hospital of Qingdao University, Qingdao 266000, China*

Received 5 June 2024; received in revised form 21 October 2024; accepted 26 November 2024

KEY WORDS

Iron overload;
Heart diseases;
Ferroptosis;
I/R;
Parkin;
ACSL4;
p53;
Mitochondrial

Abstract Iron overload is strongly associated with heart disease. Ferroptosis is a new form of regulated cell death indicated in cardiac ischemia−reperfusion (I/R) injury. However, the specific molecular mechanism of myocardial injury caused by iron overload in the heart is still unclear, and the involvement of ferroptosis in iron overload-induced myocardial injury is not fully understood. In this study, we observed that ferroptosis participated in developing of iron overload and I/R-induced cardiomyopathy. Mechanistically, we discovered that Parkin inhibited iron overload-induced ferroptosis in cardiomyocytes by promoting the ubiquitination of long-chain acyl-CoA synthetase 4 (ACSL4), a crucial protein involved in ferroptosis-related lipid metabolism pathways. Additionally, we identified *p53* as a transcription factor that transcriptionally suppressed Parkin expression in iron-overloaded cardiomyocytes, thereby regulating iron overload-induced ferroptosis. In animal studies, cardiac-specific Parkin knockout mice (*Myh6-CreER^{T2}/Parkin$^{fl/fl}$*) fed a high-iron diet presented more severe myocardial damage, and the high iron levels exacerbated myocardial I/R injury. However, the ferroptosis inhibitor Fer-1 significantly suppressed iron overload-induced ferroptosis and myocardial I/R injury. Moreover, Parkin effectively

*Corresponding author.
E-mail address: wangjx@qdu.edu.cn (Jianxun Wang).

Peer review under the responsibility of Chinese Pharmaceutical Association and Institute of Materia Medica, Chinese Academy of Medical Sciences.

https://doi.org/10.1016/j.apsb.2024.12.027

protected against impaired mitochondrial function and prevented iron overload-induced mitochondrial lipid peroxidation. These findings unveil a novel regulatory pathway involving p53−Parkin−ACSL4 in heart disease by inhibiting of ferroptosis.

1. Introduction

Iron is an indispensable trace element that plays critical roles in various biological processes, such as energy metabolism, nucleotide synthesis, and DNA repair[1,2]. However, disturbances in iron homeostasis, including iron deficiency and iron overload, can lead to various cardiovascular diseases[3-5]. Iron deficiency is the most prevalent malnutrition-related condition and affects up to 75% of patients with heart failure[6]; however, iron overload can increase the risk of cardiovascular diseases by inducing oxidative stress and lipid peroxidation, including myocardial ischemia−reperfusion (I/R) injury and myocardial infarction[7,8]. The results of clinical research have demonstrated that myocardial infarct areas exhibit an increased iron content compared with noninfarct areas, which is a risk factor for left ventricular remodeling[9]. This supposition is further supported by studies conducted in mice with cardiac I/R, in which the injection of an iron chelator during I/R resulted in a significant reduction in both acute and chronic cardiac injury[10-12]. Moreover, the use of an iron chelator protected cardiomyocytes from death induced by doxorubicin in mouse hearts[13]. Doxorubicin-induced cardiomyocyte death and cardiac dysfunction result from elevated mitochondrial iron levels, which contribute to reactive oxygen species (ROS) production and the accumulation of lipid peroxides[10]. Although numerous studies have proven the association between iron overload and cardiac diseases, the exact mechanism of iron regulation remains unknown.

Ferroptosis, a newly discovered form of iron-dependent cell death, was first identified in 2012[14]. The iron-dependent accumulation of lipid peroxides was also characterized. Excessively reactive ferrous iron accelerates the generation of ROS *via* the Fenton reaction, and these ROS interact with polyunsaturated fatty acids (PUFAs) in lipid membranes and induce lipid peroxidation, thus damaging the integrity and fluidity of cell membranes[15-17]. Current evidence suggests that the pathogenesis of cardiovascular diseases, such as diabetic cardiomyopathy, hypertrophic cardiomyopathy, anthracycline cardiotoxicity and heart failure[18-22], is linked to ferroptosis. Moreover, the overexpression of antioxidant proteins, such as glutathione peroxidase (GPX4), which is the most important negative controller of ferroptosis, has been reported to have a cardioprotective effect after I/R injury[23-25]. On the other hand, the use of iron chelation during acute and chronic myocardial I/R injury can inhibit ferroptosis in cardiomyocytes[10]. However, whether ferroptosis is involved in iron overload-induced cardiomyocyte death remains unclear.

Parkin (*PARK2*) was first identified as a Parkinson's disease-associated gene and functions as an E3 ubiquitin−protein ligase involved in the ubiquitin−proteasome-dependent pathway[26]. Parkin protects against dopaminergic cell death by blocking mitochondrial swelling and the release of cytochrome *c*[27]. Loss of Parkin function leads to mitochondrial dysfunction and increased mitochondrial fragmentation[28]. Damaged mitochondria are cleared through Parkin-mediated mitophagy. Pink1 selectively recruits Parkin to damaged mitochondria, which is crucial for mitophagy[29,30]. Parkin is highly expressed in the heart and contributes significantly to heart development[31]. Parkin deficiency inhibits postnatal mitochondrial maturation, which is critical for survival[32]. The expression level of Parkin in cardiomyocytes is downregulated in cardiac disorders such as I/R injury, hypoxia injury, diabetic cardiomyopathy, myocardial aging, and cardiac hypertrophy[33-35]. Reduced Parkin levels are associated with cardiac pathology, but the underlying mechanism needs to be further explored[33]. Thus, we were interested in whether Parkin participates in iron overload-induced cardiomyocyte ferroptosis.

In this study, we observed that iron overload-induced ferroptosis and exacerbated hypoxia-induced cardiomyocyte death. Interestingly, the overexpression of Parkin significantly inhibited iron overload-induced ferroptosis, ultimately playing a protective role in cardiomyocytes. We further revealed that Parkin exerts its anti-ferroptotic effects by ubiquitinating long-chain acyl-CoA synthetase (ACSL4), leading to a decrease in cellular lipid peroxidation. Additionally, p53 transcriptionally inhibited Parkin expression, thereby inhibiting ACSL4 ubiquitination by Parkin and inducing ferroptosis in cardiomyocytes, ultimately impairing cardiac function. Our findings reveal a novel regulatory pathway involving p53−Parkin−ACSL4 in ferroptosis, which provides innovative strategies for preventing cardiovascular diseases.

2. Materials and methods

2.1. Animals

C57BL/6J mice were purchased from Vital River Laboratory Animal Technology Co., Ltd. (Beijing, China). $Parkin^{flox/flox}$ ($Parkin^{fl/fl}$) mice were purchased from WIEWSOLID BIOTECH Co., Ltd. (VSM40086, Beijing, China). *Myh6-CreER*^{T2} mice were purchased from Cyagen Biosciences Inc. (Guangzhou, China). To generate *Myh6-CreER*^{T2}/$Parkin^{fl/fl}$ mice, we crossed $Parkin^{fl/fl}$ mice with *Myh6-CreER*^{T2} mice. To induce Cre-mediated excision, mice were injected intraperitoneally with tamoxifen (1 mg/mouse/day) at six weeks of age for seven consecutive days. Tamoxifen was prepared by solubilizing 20 mg in 1 mL peanut oil. These mice were carefully selected to ensure similar age and weight. Tamoxifen and oil were purchased from Sigma−Aldrich Co., Ltd. (Shanghai, China). Only male mice were included in the study due to the significant resistance of females to iron overload-induced cardiomyopathy[36,37].

All animals' experiments (including the euthanasia procedure) were approved by the Institutional Animal Care and Use Ethics Committee of the Medical College of Qingdao University (QDU-AEC-2021800). Mice were anesthetized with 1%−2% isoflurane inhalation and were euthanized *via* inhalation of CO_2 (100%)

followed by cervical dislocation as a secondary confirmation of death, the heart and blood were isolated and dissected for further *ex vivo* studies.

2.2. Cardiac-specific Parkin knockout mice

Myh6-CreER^{T2}/Parkin$^{fl/fl}$ and *Parkin$^{fl/fl}$* mice: *Myh6-CreER^{T2}/Parkin$^{fl/fl}$* mice were randomly divided into 2 groups: Normal diet group (50 mg iron/kg) and high iron diet group (8.3 g iron/kg), with 8 mice in each group, were fed high iron for 6 weeks and normal diet for 6 weeks. Similarly, *Parkin$^{fl/fl}$* mice were randomly divided into two groups, fed a high iron diet (HID) for 6 weeks and a normal diet for 6 weeks, respectively. After examining the mice's heart function with a small animal ultrasound machine 6 weeks after feeding, heart tissue was taken and fixed in liquid nitrogen and a 4% paraformaldehyde solution before being used for other tests.

2.3. High-iron diet and I/R myocardial injury models, along with measurement of infarct size

I/R myocardial injury and infarct size measurement: (1) 8-week-old male C57BL/6J mice were randomly assigned to 4 groups using a labeling method: Sham, Saline + I/R, HID + I/R, HID + Fer-1+ I/R, with eight mice in each group. The I/R operation was performed after 6 weeks of high iron feeding. Fer-1 (10 mg/kg) was administered *via* intraperitoneal injection 24 h and 2 h before the I/R surgery. In brief, mice were anesthetized with 1%−2% isoflurane inhalation. A left thoracotomy was performed around the third intercostal space, and the left anterior descending (LAD) coronary artery was temporarily ligated using sterile 8-0 silk suture with a slipknot. Proper ligation was confirmed by visually observing the left ventricle wall turning pale. After 30 min of regional ischemia, the heart was allowed to reperfuse, resulting in the restoration of normal color to the myocardium distal to the ligation. Sham-operated animals underwent the same procedure without ligation of the LAD coronary artery. Blood and heart samples were collected for various tests. (2) Eight-week-old male C57 BL/6J mice were randomly assigned to 3 groups using a labeling method: Sham, I/R + β-gal, and I/R + Parkin, with 8 mice in each group. In brief, mice were injected with Parkin overexpressing adenovirus or control β-gal *via* intravenous injection into the tail, after 3 weeks, the mice were subjected to sham or I/R surgery. The specific method is the same as above. Blood and heart samples were collected for various tests.

To measure the infarct size, the animals were re-anesthetized after a 24 h reperfusion period. The LAD was tightly re-occluded, and Evans blue dye was injected through the external iliac vein. After being excised and rinsed in phosphate buffer saline, the heart was frozen at −20 °C for 20 min and then cut transversely into slices (4−5 slices per heart). These slices were incubated for 20 min with a 1.5% solution of 2,3,5-triphenyl tetra-sodium chloride (TTC) to visualize the unstained infarcted region. The infarct size (IF), area at risk (AAR), and non-ischemic left ventricle were assessed and analyzed using ImageJ (NIH, USA).

2.4. Cell culture and treatment

The embryonic rat heart-derived cell line H9c2 cells were purchased from the National Collection of Authenticated Cell Cultures (Shanghai, China). H9c2 cells were cultured in Dulbecco's modified Eagle's medium (DMEM, Gibco, USA), supplemented with 10% fetal bovine serum (Royacel, China) and 1 × penicillin−streptomycin (Gibco, USA), at a temperature of 37 °C in a humidified atmosphere containing 5% CO_2 and 95% air. Neonatal rat and mice cardiomyocytes were isolated and cultured as previously described[38]. The following reagents were used to treat cells at the indicated concentrations: FAC (Ferric citrate, F5879), (E7781), ferrostatin-1 (Fer-1, 0583) and *N*-acetyl-L-cysteine (NAC, A9165) were purchased from Sigma−Aldrich Co., Ltd. (Sahnghai, China). Necrostatin-1 (Nec-1s, 8641) was purchased from Selleckchem Co., Ltd. (USA), z-VAD-FMK (zVAD, 550377) was purchased from Becton Dickinson Co., Ltd. (USA).

2.5. Measurement of iron content

An iron kit (E-BC-K880-M, Elabscience, Wuhan, China) determined the cell's total iron content. 10^6 cells were mixed with 500 μL lysate for cell samples, homogenized, fully dissolved at 4 °C, centrifuged at 10,000 × *g* for 10 min, and the supernatant was collected. An iron kit (E-BC-K772-M, Elabscience, Wuhan, China) determined the cardiac total iron content. For animal samples 0.2 g of fresh animal heart tissue was taken and homogenized at low temperature with 500 μL lysate. The supernatant was removed after centrifugation at 10,000 × *g* at 4 °C for 10 min. The 300 μL of the standard substance of different concentrations was taken into the corresponding 1.5 mL EP tube. For the determination tube, 300 μL of the sample was brought into the corresponding 1.5 mL EP tube. To each tube, 150 μL of color-developing solution was added. The mixture was incubated at 37 °C for 40 min and then centrifuged at 12,000 × *g* for 10 min. Finally, 300 μL of the supernatant from each tube was taken and added to the corresponding well of the enzyme label plate. The absorbance at 593 nm was measured using a Microplate Reader.

2.6. Measurement of cell death

Cell death was assessed using the PI kit (CA1040, Solarbio, Shanghai, China) following the manufacturer's instructions. Briefly, cardiomyocytes were seeded at a density of 8×10^3 cells per well in a 24-well plate. After the designated treatment, 500 μL of PI staining solution was added to each well. The plate was then incubated on ice in the dark for 30 min, followed by two washes with PBS. Subsequently, 500 μL of 4% paraformaldehyde was added to each well at room temperature for 1 h. Finally, DAPI was used to stain the nuclei. The nuclei were stained blue, while the dead cells were stained red. Fluorescence microscopy was utilized to capture images and determine the percentage of cell death. Three random fields were selected for each sample, and 100 cells were randomly counted in each field to calculate cell mortality.

2.7. Measurement of MDA content

Lipid peroxidation was assessed using an MDA kit (BC0025, Solarbio, Shanghai, China). The cell and tissue samples were treated with 1 mL of extraction solution, followed by sonication (power 20 W, 3 s on, 10 s off, repeated 30 times). After centrifugation at 4 °C at 8000 rpm for 10 min (Eppendorf, Germany, 5424R), the supernatant was collected and added to the MDA detection solution. The mixture was then incubated in a water bath at 100 °C for 60 min, followed by centrifugation at 10,000 × *g* for 10 min. Subsequently, 200 μL of the supernatant was transferred

to a 96-well plate. The absorbance at 450, 532, and 600 nm was measured using a Microplate Reader.

2.8. Immunoblotting

Total proteins were extracted from the cardiomyocytes or tissues by homogenizing them in RIPA buffer (Solarbio, Shanghai, China) containing protease inhibitors. The homogenate was cleared by centrifugation at 4 °C for 30 min at 12,000 rpm (Eppendorf, Germany, 5424R), and the supernatant (containing the protein fraction) was collected. Protein concentration in the supernatant was measured using the BCA Protein Assay Kit (Beyotime, Shanghai, China). A total of 20 μg protein per sample was resolved in a 12% SDS-PAGE and transferred to a nitrocellulose membrane. The membranes were blocked with 5% BSA in Tris-buffered saline containing 0.2% Tween-20, then incubated with primary antibodies at 4 °C overnight. The following antibodies were used: anti-Parkin (1:1000, #4211), anti-p53 (1:1000, #9282) and anti-β-actin (1:1000, #93473) were purchased from Cell Signaling Technology (MA, USA). Anti-ACSL4 (1:1000, Ab155282) was purchased from Abcom (MA, USA). Anti-Ptgs2 (1:1000, 12375-1-AP) and anti-actinin (1:500, 14221-1-AP) were purchased from Proteintech (Chicago, USA). Anti-GFP (1:1000, AE030), anti-Myc (1:1000, AE010), anti-HA (1:1000, AE036), anti-α-SMA (1:1000, A17910), anti-SLC7A11 (1:1000, A2413), anti-TFRC (1:1000, A5865) and anti-GPX4 (1:1000, A13309) were purchased from ABclonal Biotechnology Co., Ltd. (Beijing, China). Anti-ACSL1,3,5 (1:1000, ER60807, ER60808, ER60809), anti-CTGF (1:1000, ER1802-69), anti-NIX (1:1000, HA722056), anti-BNIP3 (1:1000, ET1704-08), anti-FUNDC1 (1:1000, ER65664), anti-LC3 (1:1000, ET1701-65) were purchased from HUABIO Biotechnology Co., Ltd. (Hangzhou, China). The membranes were then washed and probed with the appropriate horseradish peroxidase-conjugated secondary antibodies (1:5000; ABclonal) and detected using the Pierce ECL System (Cat#32106, Beijing ThermoFisher Biochemical Products Co., Ltd., Beijing, China).

2.9. Quantitative real-time PCR

Total RNA was isolated from tissues or cardiomyocytes using Trizol (Vazyme Biotech Co., Ltd., Nanjing, China), and RNA concentration and purity were measured using spectrophotometry. RNA was reverse-transcribed using the PrimeScript RT reagent Kit (Vazyme Biotech Co., Ltd., Nanjing, China) according to the manufacturer's instructions. Quantitative PCR was performed using a CFX96 Real-Time System (Bio-Rad, CA, USA) and SYBR Green Supermix (Vazyme Biotech Co., Ltd., Nanjing, China) by the manufacturer's instructions. The fold difference in gene expression was 6 calculated using the $2^{-\Delta\Delta Ct}$ method and is presented relative to *GAPDH* mRNA. All reactions were performed in triplicate, and specificity was monitored using melting curve analysis. See Supporting Information Tables S1 and S2 for the PCR primers used.

2.10. Immunoprecipitation

The cells were incubated with 500 μL NP-40 lysis buffer at 4 °C for 30 min. After centrifugation, 50 μL samples were aliquoted for input, and the remaining samples were used for immunoprecipitation. The samples were incubated with 2 μg anti-GFP or anti-Parkin antibody, and 50 μg Protein-A/G PLUS-Agarose (Shanghai Santa Cruz Biotechnology Co., Ltd., Shanghai, China), rotating at 4 °C overnight. Then, the beads were successively treated with the following steps: washing twice with 1 mL NP-40 lysis buffer, mixing with 25 μL sample buffer, and boiling for 10 min. The released proteins were subjected to 12% SDS-PAGE and detected by immunoblotting using an anti-ACSL4 antibody as described earlier.

2.11. Cell transfection

Using Lipo3000 as the transfection reagent, Parkin, PcDNA3.1, ACSL4, Parkin-siRNA, ACSL4-siRNA, p53-siRNA, and the negative control (NC) were transfected for 24 h. The siRNA of Parkin, ACSL4, and p53 were all produced by Shanghai Jima Pharmaceutical Technology Co., Ltd. (Shanghai, China). The specific sequence can be seen in Supporting Information Table S3.

Transfection system (taking one well in a six-well plate as an example):

A: 125 μL DMEM + 4 μL Lipo3000;
B: 125 μL DMEM + 5 μL P3000 + 2 μg plasmid (5−10 μL siRNA). After 5 min, the 2 tubes were mixed and let stand for 15 min, and then added to a 6-well plate.

2.12. Analysis of mitochondrial membrane potential ($\Delta\Psi m$)

$\Delta\Psi$m was measured using the sensitive fluorescent probe JC-1, a cationic dye of 5,5′,6,6′-tetrachloro1,1′,3,3′-tetraethyl benzimidazole carbocyanine iodide (C2006, Beyotime Biotechnology, Shanghai, China). Briefly, cardiomyocytes were seeded at 10^6 cells per well in a 6-well plate. After 12 h of treatment, the culture medium was poured away, and washed with cell buffer PBS 3 times. Take 50 μL JC-1 (200 ×) stock solution and dilute it with 8 mL double distilled water. The solution was thoroughly mixed, and then 2 mL of JC-1 dyeing buffer (5 ×) was added to make 10 mL JC-1 dyeing working liquid. One milliliter JC-1 dye working solution was added to each well of the 6-well plate, thoroughly mixed, and incubated in the cell incubator at 37 °C for 20 min. After incubation, the supernatant was removed, and the wells were washed twice with JC-1 staining buffer. Two milliliters of cell culture medium were added to each well. Fluorescence microscope photographs were taken and analyzed. For each sample, 3 fields were randomly selected, and 100 cells were randomly measured from each field to calculate mitochondrial membrane potential.

2.13. Measurement of mitochondrial iron

Mito-Ferro Green probe (M489, DOJINDO, Japan) was used to detect mitochondrial iron levels. In brief, cardiomyocytes were seeded at 8×10^3 cells per well in a 24-well plate. After the indicated treatment, the culture medium was poured away, and washed with cell buffer PBS 3 times, 5 μmol/L Mito-FerroGreen and 1 μmol/L mitotracker, a mitochondrial staining probe, were mixed and added into each well. Then analyzed immediately with the LSM-710 confocal microscope (Leica, Germany). For each slide, 3 different fields were selected randomly to acquire images and 20 mitochondria were examined in each field.

2.14. Measurement of mitochondrial oxygen consumption

Mitochondrial oxygen consumption in cardiomyocytes was measured using the Seahorse kit (103015-100, Agilent Technologies, Shanghai, China). In brief, cardiomyocytes were seeded at 2500 cells per well in the XFp cell culture plate. After the indicated treatment, the probe plate was hydrated and the whole probe plate device was incubated overnight in a CO_2-free cell incubator at 37 °C. The test working liquid is added into the corresponding dosing hole of the probe plate in turn in the corresponding volume and detected by the Seahorse instrument.

2.15. Measurement of mitochondrial lipid ROS

Cardiomyocytes were seeded at 8×10^3 cells per well in a 24-well plate. After the indicated treatment, the culture medium was poured away and washed with cell buffer PBS 3 times, cells were stained in a 37 °C incubator for 30 min with 0.03 μmol/L MitoTracker Red CMXRos (Molecular Probes) and 1 μmol/L C11-BODIPY (581/591) (Invitrogen, CA, USA). After staining, the cells were washed 3 times with PBS, 500 mL of 4% paraformaldehyde was added at room temperature for 1−2 h, and then the nuclei were stained with DAPI. Then analyzed immediately with the LSM-710 confocal microscope. For each sample, three fields were randomly selected and 20 mitochondria were examined in each field.

2.16. Measurement of ATP

The ATP test kit (S0026, Beyotime Biotechnology, Shanghai, China) was used to detect ATP levels in cardiomyocytes. In brief, each well of the 6-well plate was added 200 μL of lysate. Following cell lysis, samples were subjected to centrifugation at 12,000 × *g* for 5 min at 4 °C. The supernatant was collected, and 100 μL of ATP detection working solution was added to the detection well, which was then incubated at room temperature for 3−5 min. Subsequently, 20 μL of either sample or standard was added to the detection well or tube, and the RLU value was measured using a Microplate Reader.

2.17. Measurement of creatine kinase isoenzyme (CK-MB) content

The CK-MB test kit (H197-1-2, Nanjing Jiancheng Bioengineering Institute, Nanjing, China) was used to detect CK-MB content. In brief, 50 μL of standard solution and 50 μL of biotin antigen working solution were added to each well of a 96-well plate, followed by sealing with an adhesive film and incubation at 37 °C for 30 min. Each well was then washed five times with 200 μL of washing buffer, allowing 30 s per wash, and subsequently patted dry. Next, 50 μL of avidin-HRP was added to each well, gently mixed, resealed, and incubated at 37 °C for 30 min. After repeating the washing step as described above, 50 μL of color developing solution A and 50 μL of color developing solution B were added to each well, covered, and allowed to develop color in the dark for 10 min. Finally, 50 μL of stop solution was added to each well, and the OD value at 450 nm was measured using a Microplate Reader.

2.18. Measurement of cardiac cell death

100 μL PI dye (10 mg/kg) was injected into the pulmonary veins of mice to label dead cells. The following operations are all in the dark. The heart was taken out and frozen in liquid nitrogen to prepare tissue slices with a thickness of 6 μm. Sections were washed 3 times with 1 × PBS for 3−5 min each, followed by blocking in 3% BSA at room temperature for 1 h. Primary antibody actinin was incubated overnight at 4 °C. After washing 3 times with PBS for 5 min each, sections were incubated with the secondary antibody (Alexa Fluor 488 Goat Anti-Rabbit IgG) for 1 h at room temperature. Sections were washed again 3 times with PBS for 5 min each, and nuclei were stained with DAPI. Samples were observed and analyzed under fluorescence microscopy. Five random fields were selected from each sample, and 100 cells were randomly counted in each field to calculate the percentage of cell death.

2.19. Lipidomic analysis

Collect and process cardiomyocytes (1×10^7) following the protocol of BioProfile Technology (Shanghai, China). Lipidomic profiling was conducted using the ultraperformance liquid chromatography−mass spectrometry system (Q Exactive Plus, Thermo Scientific) at Shanghai BioProfile Biotechnology. The mass spectrometric data were analyzed using the Lipid Search 4.1.30 software (Thermo Scientific, USA).

2.20. Adenoviral construction

Parkin adenoviral construction was prepared as described previously[39]. Briefly, the rat Parkin gene was reverse-transcribed from total RNA isolated from the rat heart, and then inserted into the Adeno-XTM expression system (Clontech Laboratories, Mountain View, CA, USA) in line with the manufacturer's guidelines. The adenovirus containing β-galactosidase (β-gal) was prepared as the control. RFP−GFP−LC3 adenoviral was purchased from the Shanghai Hanheng Biological Technology (Shanghai, China). All constructs were produced and amplified in HEK293T cells. H9c2 cells were infected with adenoviruses at 180 multiplicity of infection in the absence of FBS for 5 h.

2.21. Chromatin immunoprecipitation (ChIP)

ChIP can be used for probing protein−DNA interactions. The experiment was conducted as previously described[40]. Briefly, cells were fixed with formaldehyde to cross-link histone and non-histone proteins to DNA. After cross-linking, chromatin can be fragmented into 100−300 bp pieces through ultrasound to facilitate target protein exposure. Immunoprecipitation is executed at 4 °C employing p53 and IgG antibodies, then heated at 65 °C for 6 h to disrupt the formaldehyde crosslinks. DNA fragments were purified with a Beyotime DNA Gel Extraction Kit (Shanghai, China). Purified DNA was analyzed by quantitative real-time PCR, using the primers that encompass p53 of the Parkin promoter. The sequence of ChIP-PCR primers:

Forward: TCATCATGGCTTTGACTGTGAAG;
Reverse: GGAAGATGGTGGCAGAAAAAGA.

2.22. Surface plasmon resonance (SPR) analysis

Recombinant Parkin and ACSL4 proteins were used in SPR analysis with a Biacore T200 instrument (Biacore, Uppsala, Sweden). The protein's amino group was connected to the activated carboxyl group on the CM5 chip. Initially, ACSL4 was thinned to 20 μg/mL in 200 μL of 10 mmol/L sodium acetate at pH 5 and then streamed over the activated CM5 sensor chip surface for binding. The remaining activated sites on the CM5 sensor chip were blocked with 1 mol/L ethanolamine at pH 8.5. Various concentrations of Parkin (2.5, 5, 10, and 20 μg/mL) in 20 mmol/L Tris-HCl buffer at pH 7.4 were used to analyze the interactions.

2.23. Statistical analysis

Data were analyzed and graphed using GraphPad Prism 8.0 software (La Jolla, CA, USA), and are presented as mean ± standard error of the mean (SEM). Paired data were evaluated by Student's *t*-test. We used a one-way ANOVA for multiple comparisons. A value of $P < 0.05$ was considered significant.

3. Results

3.1. Iron overload induces cardiomyocyte ferroptosis and promotes cell death caused by hypoxia-reoxygenation (H/R) in vitro

The effects of iron overload on cardiomyocytes were evaluated by treating cardiomyocytes with FAC. Dose-dependent increases in cell death and iron content were observed in H9c2 cells and neonatal rat cardiomyocytes (Fig. 1A and B, Supporting Information Fig. S1A and S1B). FAC treatment also induced a robust increase in the lipid peroxidation product MDA (Fig. 1C and Fig. S1C) and in the mRNA and protein levels of *Ptgs2* (Fig. 1D and E, Fig. S1D), a putative molecular marker of ferroptosis, indicating the involvement of ferroptosis in iron overload-induced cell death[41]. The impact of iron overload-induced cell death was further investigated by employing various cell death inhibitors to assess cell viability following treatment with 100 μmol/L FAC. The results reveal that ferroptosis inhibitors, such as ferrostatin-1 (Fer-1), reversed cell death (Fig. 1F) and the changes in the MDA content (Fig. 1G) and the *Ptgs2* mRNA level (Fig. 1H). In contrast, other forms of cell death inhibitors, including necrostatin-1 (a necroptosis inhibitor) and ZVAD (an apoptosis inhibitor), did not significantly alleviate cell death or lipid peroxidation (Fig. 1F−H). These data indicate that iron overload primarily induced cardiomyocyte death through the ferroptosis pathway.

Iron overload can increase the risk of cardiovascular disease and increase cellular iron levels in damaged cardiomyocytes[42,43]. Treatment of cardiomyocytes with H/R led to an increase in iron levels (Fig. 1I and Fig. S1E). Cardiomyocytes were treated with a low concentration of FAC (25 μmol/L), followed by H/R. Iron significantly exacerbated H/R-induced cell death (Fig. 1J) and decreased the MDA concentration (Fig. 1K). Interestingly, the ferroptosis inhibitor Fer-1 significantly reduced these effects (Fig. 1J and K). These data demonstrate that inhibiting ferroptosis reduced iron-induced cell injury from H/R.

3.2. Parkin inhibits ferroptosis induced by iron overload in vitro

However, whether Parkin participates in iron overload-induced ferroptosis in cardiomyocytes is unclear. First, we measured Parkin expression in cardiomyocytes exposed to 100 μmol/L FAC. Strikingly, both the mRNA and protein levels of Parkin decreased in a time-dependent manner (Fig. 2A and B). The expression level of Parkin was also determined in mice fed a high-iron diet (HID) and we found that the expression level of Parkin was lower in the hearts of HID-fed mice than in those of normal diet-fed mice group (Fig. 2C). However, treatment with the ferroptosis inhibitor Fer-1 or the iron chelator deferoxamine (DFO) effectively suppressed the reduction in Parkin levels (Supporting Information Fig. S2A). To determine the role of Parkin in iron overload-induced ferroptosis, we induced Parkin expression in cardiomyocytes *via* a constructed plasmid (Fig. 2D) and a high concentration (100 μmol/L) of FAC. The results reveal that the forced expression of Parkin reduced cell death, as indicated by a decrease in the number of PI-positive cells (Fig. 2E and F), and the MDA content (Fig. 2G) in cardiomyocytes treated with FAC. Notably, the same results were obtained in neonatal rat cardiomyocytes (Fig. S2C−S2E). Additionally, we found that FAC treatment led to increases in the levels of transferrin receptor 1 (TFRI) and ACSL4, while decreasing the levels of GPX4 and having no significant effect on solute carrier family 7a member 11 (SLC7A11); however, the overexpression of Parkin inhibited ACSL4 levels and had no impact on other ferroptosis-related proteins (Fig. 2H and Fig. S2B).

Cardiomyocytes were treated with low-dose FAC to determine whether the knockdown of Parkin sensitized the cardiomyocytes to the FAC treatment. The cell death ratio was much lower under these conditions. Knockdown of endogenous Parkin (Fig. 2I) significantly increased iron overload-induced ferroptosis (Fig. 2J and K). To further explore the role of Parkin in ferroptosis, we treated cardiomyocytes with the ferroptosis inducer erastin. We found that the protein levels of Parkin decreased with erastin treatment, and that forced expression of Parkin reversed erastin-induced ferroptosis (Fig. S2F−S2H). These findings indicate that Parkin suppressed iron overload-induced ferroptosis in cardiomyocytes.

3.3. Parkin suppresses iron overload-induced mitochondrial dysfunction

Ferroptosis-induced lipid peroxidation is primarily mediated by the excessive production of ROS in mitochondria. Therefore, we investigated the impact of Parkin on mitochondrial function in cardiomyocytes in the presence of FAC. First, we measured mitochondrial iron levels *via* Mito-FerroGreen staining and observed an increase in the mitochondrial iron content upon iron treatment of cardiomyocytes (Supporting Information Fig. S3A). We wanted to know whether an increase in the mitochondrial iron content impairs mitochondrial function. Thus, we assessed indicators of mitochondrial function, including the mitochondrial membrane potential ($\Delta\Psi m$), mitochondrial ATP, mitochondrial oxygen consumption and mitochondrial lipid ROS. Our results reveal a significant reduction in the mitochondrial membrane potential, mitochondrial ATP, and mitochondrial oxygen consumption, as well as increased mitochondrial lipid ROS and mitochondrial ROS upon iron treatment (Fig. S3B−S3F). However, both Parkin and Fer-1 treatments reversed these effects (Fig. S3B−S3F). Therefore, these findings indicate that the

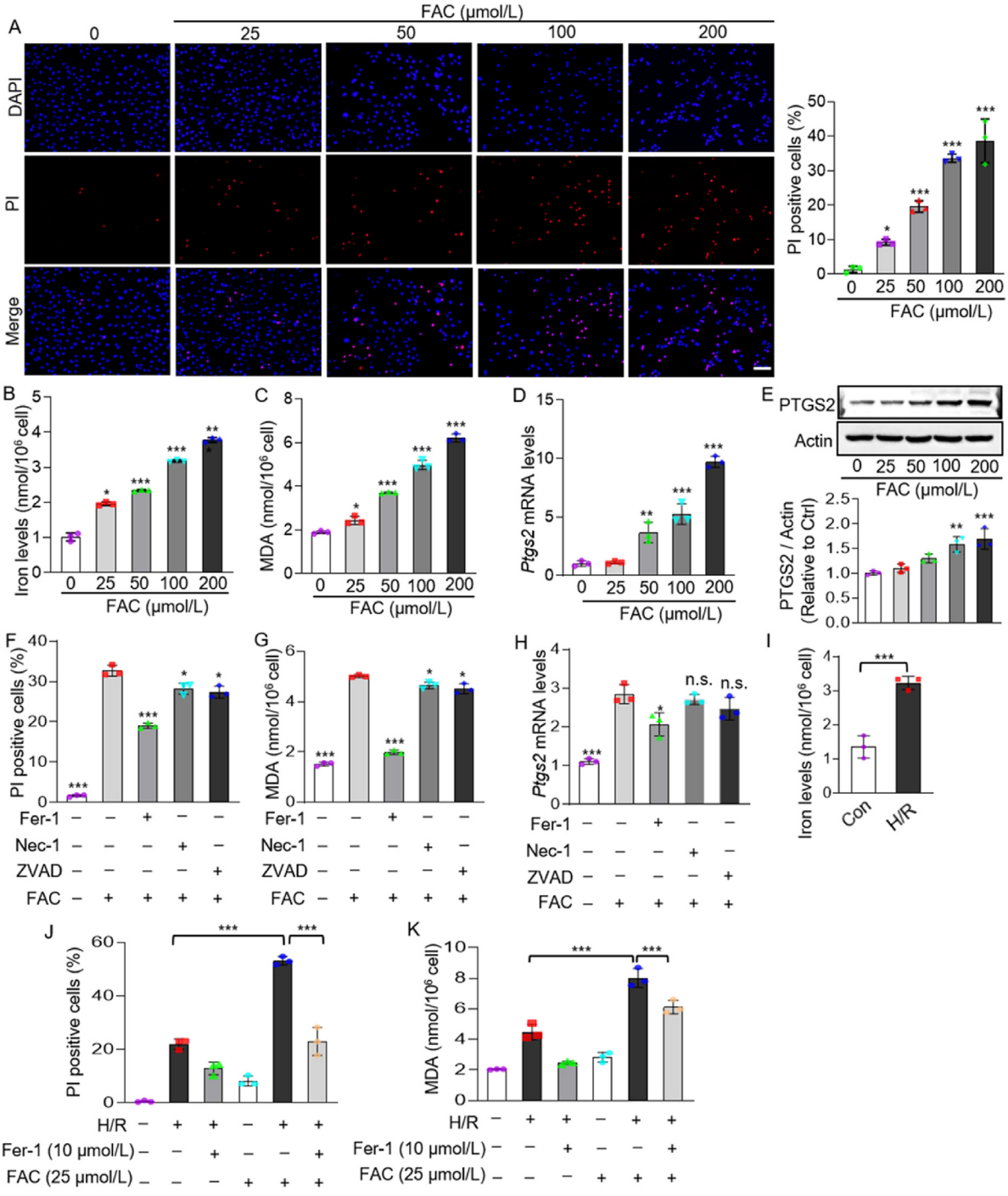

Figure 1 Iron overload induced cardiomyocyte ferroptosis and promoted hypoxic-reoxygenation (H/R)-induced cell death. (A−D) Cardiomyocytes H9c2 were treated with ferric ammonium citrate (FAC) at the indicated concentration. (A) Cell death was detected using PI staining assay. Representative images of PI-stained cells indicating cell death are shown on the left, and quantitative analysis of PI-positive cells is shown on the right. PI-positive myocyte nuclei are shown in red, while DAPI-stained nuclei are shown in blue. Scale bar: 100 μm. (B) Iron levels were measured using an iron detection reagent assay. (C) Lipid peroxidation was measured using an MDA reagent assay. (D, E) *Ptgs2* mRNA and PTGS2 protein levels were measured using RT-PCR and immunoblot, quantification is shown in the lower panel. (F−H) Cardiomyocytes were treated with the ferroptosis inhibitor Fer-1 (10 μmol/L), necrosis inhibitor Nec-1 (1 μmol/L), and apoptosis inhibitor ZVAD (5 μmol/L) for 6 h, followed by treatment with 100 μmol/L FAC for 24 h. (F) Cell death was detected using PI staining assay. (G) Lipid peroxidation was measured using an MDA reagent assay. (H) *Ptgs2* mRNA levels were measured using RT-PCR. (I−K) Iron treatment affected hypoxic−reoxygenation (H/R)-induced cardiomyocyte ferroptosis. Cardiomyocytes were hypoxic for 6 h and reoxygenated for 6 h. (I) Iron levels were measured using an iron detection reagent assay. Cardiomyocytes were treated with Fer-1 (10 μmol/L) for 6 h, and then treated with 25 μmol/L FAC for 24 h, followed by anoxic culture for 6 h and reoxygenation for 6 h. (J) Cell death was detected using PI staining assay. (K) Lipid peroxidation was measured using an MDA reagent assay. Data are presented as mean ± SD, $^{*}P < 0.05$; $^{**}P < 0.01$; $^{***}P < 0.001$ significant, one-way ANOVA, $n = 3$.

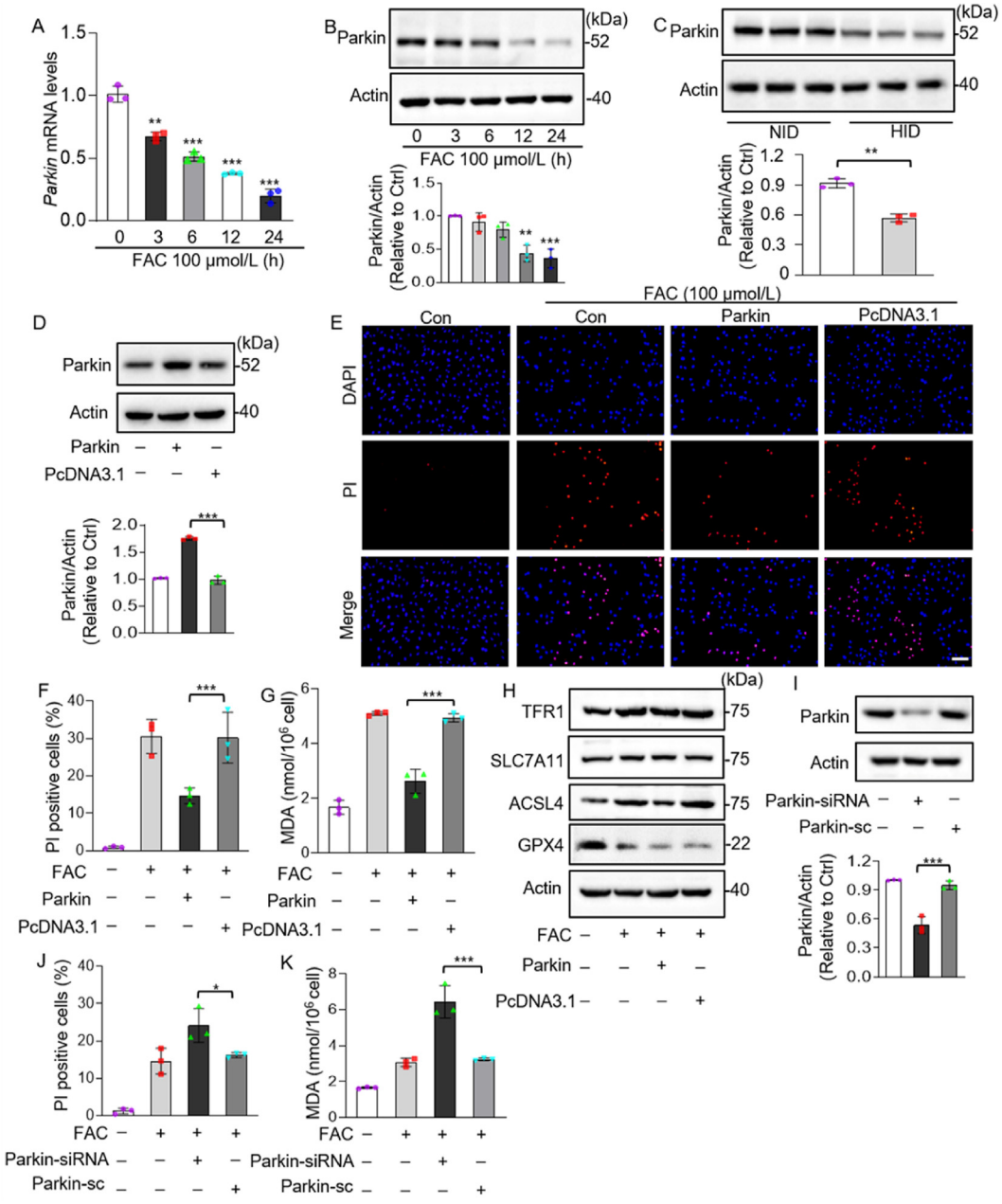

Figure 2 Parkin inhibits ferroptosis induced by iron overload *in vitro*. (A, B) Cardiomyocytes H9c2 were treated with 100 μmol/L FAC at the indicated time, and the levels of *Parkin* mRNA (A) and protein (B) were detected using RT-PCR and immunoblot, quantification is shown in the lower panel. (C) C57BL/6 mice were fed with a high iron diet for 8 weeks, while control mice were fed a regular diet. Immunoblot was performed to measure the levels of Parkin protein, quantification is shown in the lower panel. $n = 6$ mice in each group. (D) The protein levels of Parkin were analyzed using immunoblot in cardiomyocytes that were transfected with a Parkin overexpression plasmid or a control plasmid (PcDNA3.1) for 24 h. (E−G) Cardiomyocytes were treated with 100 μmol/L FAC after transfection of Parkin overexpression plasmid or a control plasmid (PcDNA3.1) for 24 h. (E) Representative images of PI staining for cell death, (F) the quantitative analysis of PI-positive cells. PI-positive myocyte nuclei are shown in red, while DAPI-stained nuclei are shown in blue. Scale bar: 100 μm. (G) Lipid peroxidation was detected using the MDA reagent assay. (H) The levels of TFR1, SLC7A11, ACSL4 and GPX4 protein were detected using immunoblot. (I) The protein levels of Parkin were analyzed using immunoblot in cardiomyocytes that were transfected with a Parkin siRNA or a control SC for 24 h, quantification is shown in the lower panel. (J, K) Knockdown of Parkin through siRNA increased iron overload-induced cell death (J) and lipid peroxidation (K) in cardiomyocytes treated with 50 μmol/L FAC for 24 h. The data are presented as mean ± SD, $^{*}P < 0.05$; $^{**}P < 0.01$; $^{***}P < 0.001$ significant, one-way ANOVA. $n = 3$.

overexpression of Parkin inhibited iron overload-induced mitochondrial damage.

The importance of Parkin in mitophagy has been reported in many works[44]. However, whether Parkin participates in iron overload-induced mitophagy in cardiomyocytes is unclear. Cardiomyocytes were infected with an adenovirus expressing RFP−GFP−LC3. FAC treatment significantly decreased both the number of green and red puncta, but overexpression of Parkin reversed these effects (Fig. S3G). The overexpression of Parkin also resulted in a significant increase in LC3 levels (Fig. S3H). These results suggest that Parkin stimulated mitophagy flux during iron overload, which may contribute to its protective effects in FAC-treated cardiomyocytes. Furthermore, FAC treatment led to a decrease in the levels of mitophagy-related proteins (NIX, BNIP3, and FUNDC1), independently of Parkin (Fig. S3I).

3.4. Parkin regulates PUFA phospholipid metabolism induced by iron overload

Ferroptosis is caused by lipid peroxidation, and PUFA-phospholipids in the cell membrane are the primary lipids prone to oxidation. Notably, previous studies have shown that phospholipids with PUFAs are more susceptible to oxidation than those with saturated fatty acids[45]. Therefore, we speculated that Parkin can regulate PUFA-lipid metabolism to inhibit iron overload-induced ferroptosis in cardiomyocytes. We conducted a lipidomic analysis of cardiomyocytes treated with or without FAC and measured the levels of the main phospholipid components in the cell membranes. The revealed showed that the phosphatidylethanolamine (PE) concentration increased in the cells treated with FAC (Fig. 3A). However, there was no significant change in

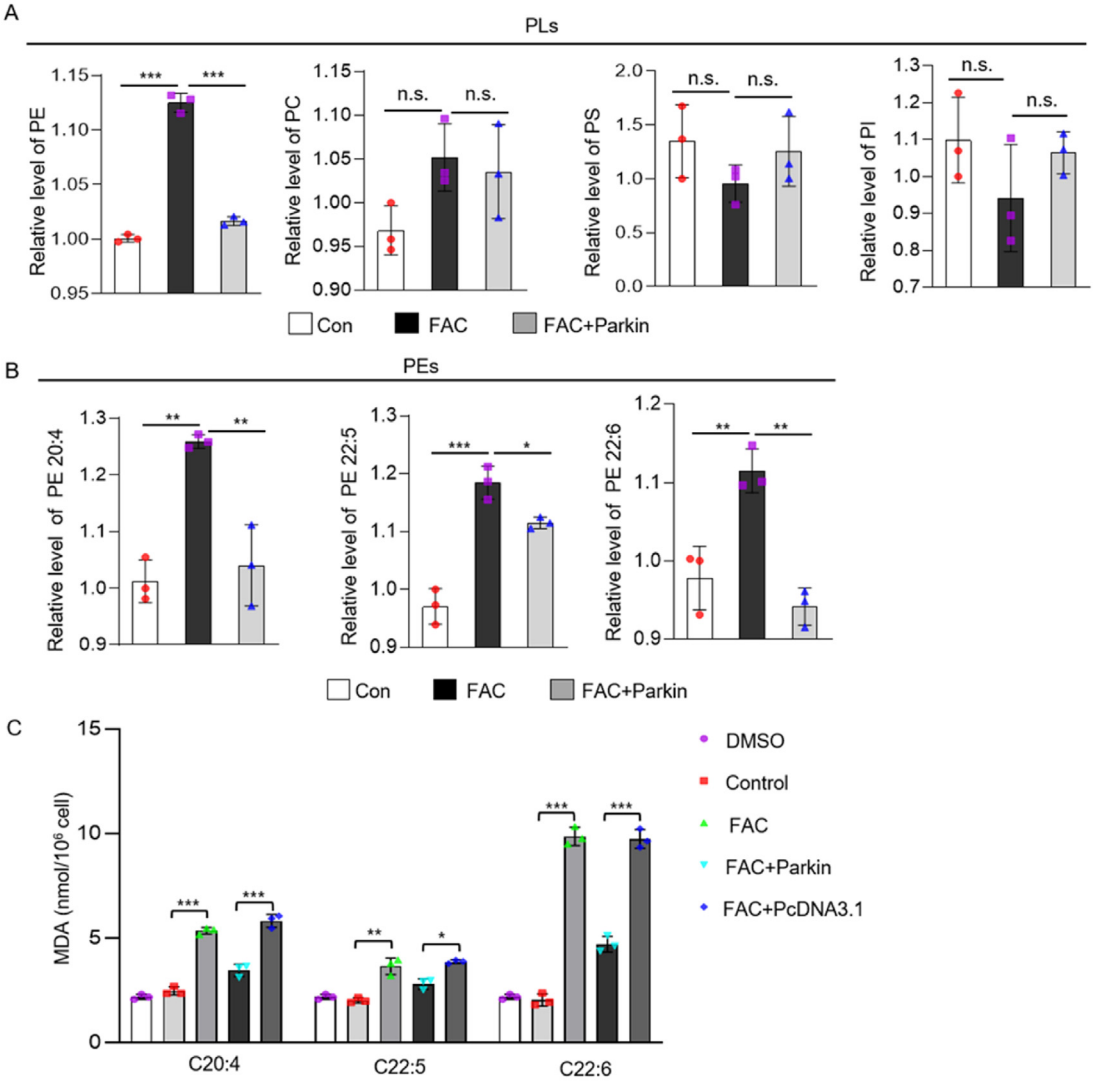

Figure 3 Parkin regulates PUFA-phospholipids metabolism induced by iron overload. (A, B) Cardiomyocytes H9c2 were treated with 100 μmol/L FAC after transfection of Parkin overexpression plasmid 24 h. (A) Lipid composition and (B) PUFAs content in lipids were detected by lipomic analysis. (C) Cardiomyocytes were treated with C20:4, C22:5, C22:6 and 100 μmol/L FAC for 24 h after transfection of Parkin overexpression plasmid and control plasmid PcDNA3.1 24 h, samples were collected to detect lipid MDA levels. Data are expressed as mean ± SD, $^{*}P < 0.05$; $^{**}P < 0.01$; $^{***}P < 0.001$ significant. n.s., not significant, one-way ANOVA. $n = 3$.

the levels of other phospholipids (phosphatidylcholine, PC; phosphatidylserine, PS; or phosphatidylinositol, PI) (Fig. 3A). Interestingly, the overexpression of Parkin significantly inhibited the iron overload-induced increase in PE levels (Fig. 3A). We subsequently examined which types of PUFAs (eicosatetraenoic acid, C20:4; docosahexaenoic acid, C22:5; and docosahexaenoic acid, C22:6) in PE significantly changed after FAC treatment. We found that the concentrations of PE that contained eicosatetraenoic acid (C20:4), docosahexaenoic acid (C22:5), and docosahexaenoic acid (C22:6) significantly increased in H9c2 cells after FAC treatment (Fig. 3B and upporting Information Fig. S4A−S4C). However, the overexpression of Parkin significantly inhibited these effects (Fig. 3B and Fig. S4A−S4C), suggesting that Parkin can regulate PUFA-phospholipid metabolism induced by iron overload. We also performed *in vitro* experiments to investigate the potential of these PUFAs in inducing ferroptosis in cardiomyocytes. We found that adding these PUFAs alone did not result in the production of MDA (Fig. 3C). However, in the presence of FAC, a significant increase in MDA production was observed in cardiomyocytes (Fig. 3C). However, Parkin protected FAC-treated cardiomyocytes from MDA production (Fig. 3C). These findings indicate that the protective effect of Parkin in the presence of FAC was most likely mediated by its regulation of the PUFA distribution in phospholipids in cardiomyocytes.

3.5. *Parkin regulates ferroptosis sensitivity by shaping the cellular lipid composition through ACSL4*

ACSL4 is known to regulate lipid biosynthesis, particularly through the preferential oxidation of PE, which contains eicosatetraenoic acid[45]. Therefore, we postulated that Parkin may modulate iron-induced PE formation and increase the PUFA content in PE by targeting ACSL4. Through lipidomic analysis, we observed that the knockdown of ACSL4 inhibited the increase in PE caused by iron overload (Fig. 4A), and the levels of PUFAs (C20:4, C22:5, and C22:6) in PE also decreased significantly (Fig. 4B). The levels of other phospholipids or PUFAs in phospholipids were unchanged or elevated (Supporting Information Fig. S5A−S5D). These findings confirm that ACSL4 mediated the incorporation of polyunsaturated fatty acids into PE.

Next, we explored the function of ACSL4 in ferroptosis. We observed that ACSL4 protein levels increased in a time-dependent manner in response to FAC and erastin treatment (Fig. 4C and Fig. S5E). The knockdown of ACSL4 (Fig. 4D) significantly inhibited iron-induced cell death (Fig. 4E) and lipid peroxidation (Fig. 4F). Furthermore, we investigated whether Parkin regulates ferroptosis in cardiomyocytes by targeting ACSL4. The overexpression of Parkin decreased the expression of ACSL4 (Fig. 4G). Other ACSLs, such as ACSL1, ACSL3, and ACSL5, were not affected (Fig. S5F). We wondered whether Parkin regulated ferroptosis in cardiomyocytes by targeting ACSL4. The overexpression of Parkin inhibited cell death (Fig. 4I) and MDA concentration (Fig. 4J) induced by FAC; however, this effect was significantly attenuated by ACSL4 overexpression (Fig. 4H−J). Therefore, these results prove that Parkin regulated iron-induced lipid metabolism by acting on ACSL4 in the context of ferroptosis.

3.6. *Parkin binds to ACSL4 and catalyzes its ubiquitination*

In subsequent experiments, we explored the molecular mechanism by which Parkin acts on ACSL4. We transfected HEK-293T cells with Myc-ACSL4, GFP-Parkin, or GFP plasmids to assess whether exogenous Parkin interacts with ACSL4, the results indicated that Parkin interacts with ACSL4 (Fig. 5A). Next, we investigated whether endogenous Parkin interacts with endogenous ACSL4. When Parkin was overexpressed in cardiomyocytes, endogenous Parkin significantly bound to ACSL4, and the overexpression of Parkin led to an increase in the immunoprecipitation of ACSL4 in H9c2 cells and neonatal rat cardiomyocytes (Fig. 5B and Supporting Information Fig. S6A). Additionally, the amount of ACSL4 immunoprecipitated by Parkin was notably decreased in cardiomyocytes treated with FAC (Fig. 5C). Hence, these findings suggest that Parkin can bind to ACSL4. Furthermore, surface plasmon resonance (SPR) revealed experiments that Parkin directly interacted with ACSL4 (Fig. 5D).

Previous studies have shown that Parkin acts as an E3 ubiquitin-protein ligase in ubiquitin proteasome-dependent pathway[24]. We investigated whether Parkin ubiquitinates ACSL4. The endogenous and exogenous ubiquitination experiments demonstrated that the overexpression of Parkin significantly enhanced the ubiquitination and degradation of ACSL4 (Fig. 5E and F), but treatment with the proteasome inhibitor MG132 inhibited the ubiquitination-mediated degradation of ACSL4 (Fig. S6B). We then examined whether FAC inhibits ACSL4 ubiquitination. Cardiomyocytes were transfected with vectors expressing HA-ubiquitin and treated with FAC. Immunoprecipitation analysis revealed indicated a decrease in the level of ACSL4 ubiquitination in response to FAC treatment (Fig. S6C), but treatment with the proteasome inhibitor MG132 reversed this effect (Fig. S6D). K48- and K63-linked polyubiquitination are two common types of polyubiquitination[46]. Therefore, we investigated which type of polyubiquitination is triggered by Parkin. The results showed that Parkin polyubiquitinated ACSL4 *via* wild-type or K48 ubiquitin but not K63 ubiquitin (Fig. 5G). These results suggest that Parkin primarily induced the polyubiquitination of ACSL4 through K48-linked ubiquitin chains. In contrast, the Parkin E3 ligase-defective mutant had a negative effect on ACSL4 ubiquitination (Fig. S6E) and failed to protect against FAC and H/R induced ferroptosis (Fig. S6F and S6G).

3.7. *p53 targets Parkin to regulate iron overload-induced ferroptosis*

p53 is a transcription factor that regulates the expression of Parkin[47]. To determine whether Parkin is a transcriptional target of *p53*, we first analyzed the consensus binding sites in the promoter regions of mouse, human and rat Parkin according to the website prediction consensus binding site of p53. The *Parkin* promoter region contains one optimal p53 binding site (−469 to −452, ATCTTGTCTGGGCATTTG) (Fig. 6A). Furthermore, a ChIP assay was used to detect whether p53 can associate with the *Parkin* promoter *in vivo*. The results reveal that p53 bound to the *Parkin* promoter region (Fig. 6B), but the knockdown of p53 decreased these effects (Fig. 6B), indicating that p53 regulates *Parkin* at the transcriptional level. To determine the role of p53 in iron overload-induced ferroptosis, we treated cardiomyocytes with FAC and observed increases in the levels of p53 mRNA (Fig. 6C) and protein (Fig. 6D and E). Furthermore, adenovirus-mediated overexpression of p53 substantially reduced the mRNA level of Parkin (Fig. 6F−H). Additionally, p53 knockdown (Fig. 6I) inhibited FAC-induced cell death (Fig. 6J) and lipid peroxidation (Fig. 6K), but when Parkin was simultaneously knocked down, these effects were reversed (Fig. 6J and K). These findings suggest that p53 promoted iron overload-induced ferroptosis in cardiomyocytes by regulating the transcription of Parkin.

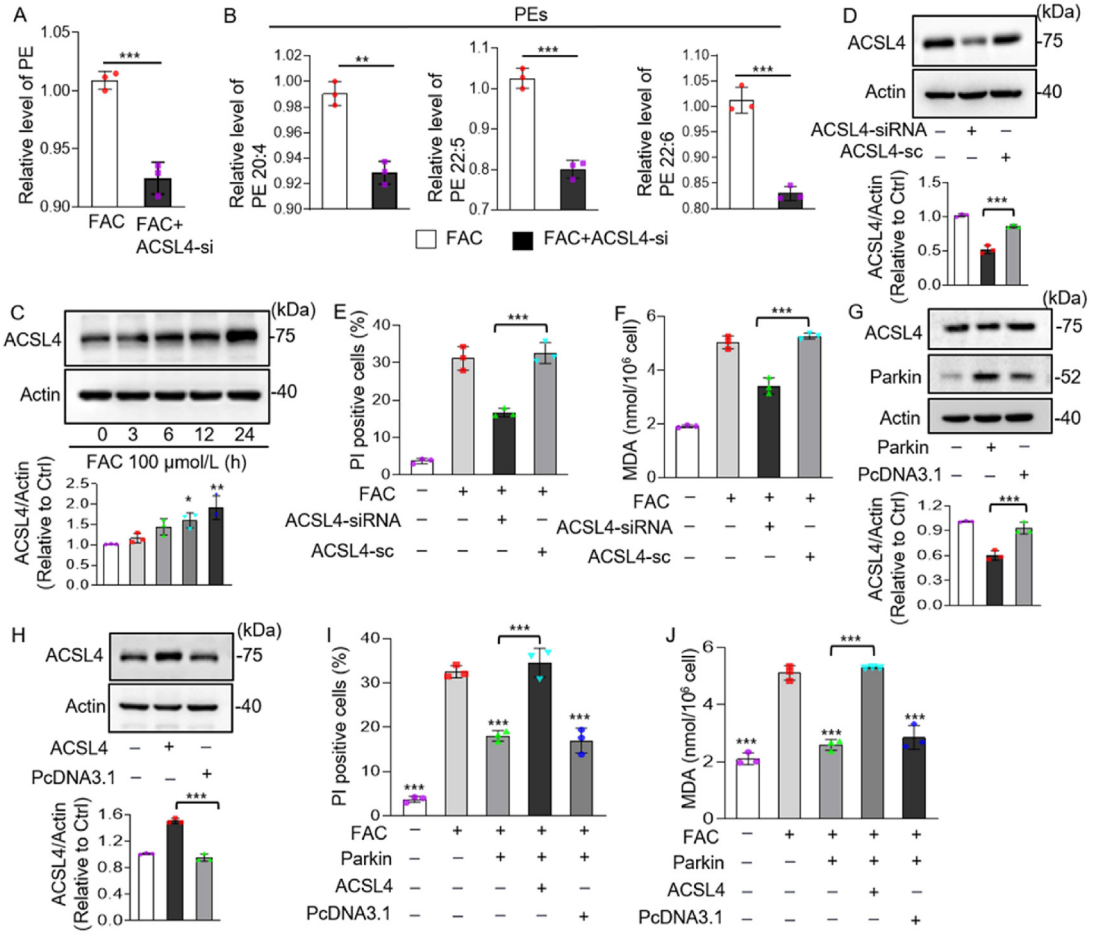

Figure 4 Parkin regulates ferroptosis sensitivity by shaping cellular lipid composition through ACSL4. (A, B) Cardiomyocytes H9c2 were treated with 100 μmol/L FAC after transfection of ACSL4-siRNA for 24 h. Student's *t*-test. $n = 3$. (A) Lipid composition and (B) polyunsaturated fatty acid content in lipids were detected by lipomic analysis. (C) Cardiomyocytes were treated with 100 μmol/L FAC at the indicated time, ACSL4 protein levels were detected by immunoblot, quantification is shown in the lower panel. (D−F) Cardiomyocytes were treated with 100 μmol/L FAC after transfection of ACSL4-siRNA for 24 h. (D) The protein levels of ACSL4 were analyzed by immunoblot, quantification is shown in the lower panel. (E) Cell death was detected by PI staining, (F) lipid peroxidation was detected by MDA reagent, one-way ANOVA. $n = 3$. (G) Enforced expression of Parkin inhibited ACSL4 protein levels by transfected with a Parkin overexpression plasmid or a control plasmid (PcDNA3.1) for 24 h in cardiomyocytes, quantification is shown in the lower panel. (H) The protein levels of ACSL4 were analyzed using immunoblot in cardiomyocytes that were transfected with ACSL4 overexpression plasmid or a control plasmid (PcDNA3.1) for 24 h, quantification is shown in the lower panel. (I, J) Enforced expression of Parkin inhibited cell death (I) and lipid peroxidation (J) in cardiomyocytes exposed to 100 μmol/L FAC, which was attenuated by overexpression of ACSL4. Data are expressed as mean ± SD, $*P < 0.05$; $**P < 0.01$; $***P < 0.001$ significant, one-way ANOVA. $n = 3$.

3.8. Iron-overloaded Myh6-CreER^{T2}/Parkin$^{fl/fl}$ mice exhibit elevated levels of tissue ferroptosis and myocardial injury

To investigate the role of Parkin in an iron overload model, we constructed cardiac-specific *Parkin* knockout mice (*Myh6-CreER^{T2}/Parkin$^{fl/fl}$*). We induced the *Myh6-Cre*-driven myocyte-specific deletion of Parkin by crossing *Parkin$^{flox/flox}$* mice with *Myh6-Cre* transgenic mice, yielding *Myh6-CreER^{T2}/Parkin$^{fl/fl}$* and *Parkin$^{fl/fl}$* (control) offspring. To induce *Cre*-mediated excision, *Myh6-CreER^{T2}/Parkin$^{fl/fl}$* mice were injected intraperitoneally with tamoxifen at 6 weeks of age for 7 consecutive days. Next, we induced iron overload in the mice by feeding them a high-iron diet for 6 weeks (Fig. 7A). Parkin was specifically depleted in the heart compared with that in *Parkin$^{flox/flox}$* mice, but was not depleted in the liver, or spleen, lungs, or kidneys (Supporting Information Fig. S7A and S7B). Furthermore, compared with mice fed a regular diet, mice fed a high-iron diet presented lower Parkin protein levels, leading to a reduction in the level of ACSL4 ubiquitination (Fig. 7B). Importantly, the *Myh6-CreER^{T2}/Parkin$^{fl/fl}$* mice also exhibited the inhibition of Parkin-mediated ACSL4 ubiquitination (Fig. 7B). We then examined whether iron overload induces ferroptosis *in vivo*. Our experiments revealed that the group fed a high-iron diet presented increased iron content (Fig. 7C and D), myocardial cell death (Fig. 7C−E), *Ptgs2* mRNA levels (Fig. 7F) and MDA content (Fig. 7G) compared with those in the usual diet group, suggesting that iron overload can induce ferroptosis *in vivo*. Importantly, the iron overload-induced ferroptosis in *Myh6-CreER^{T2}/Parkin$^{fl/fl}$* mice worsened (Fig. 7C−G).

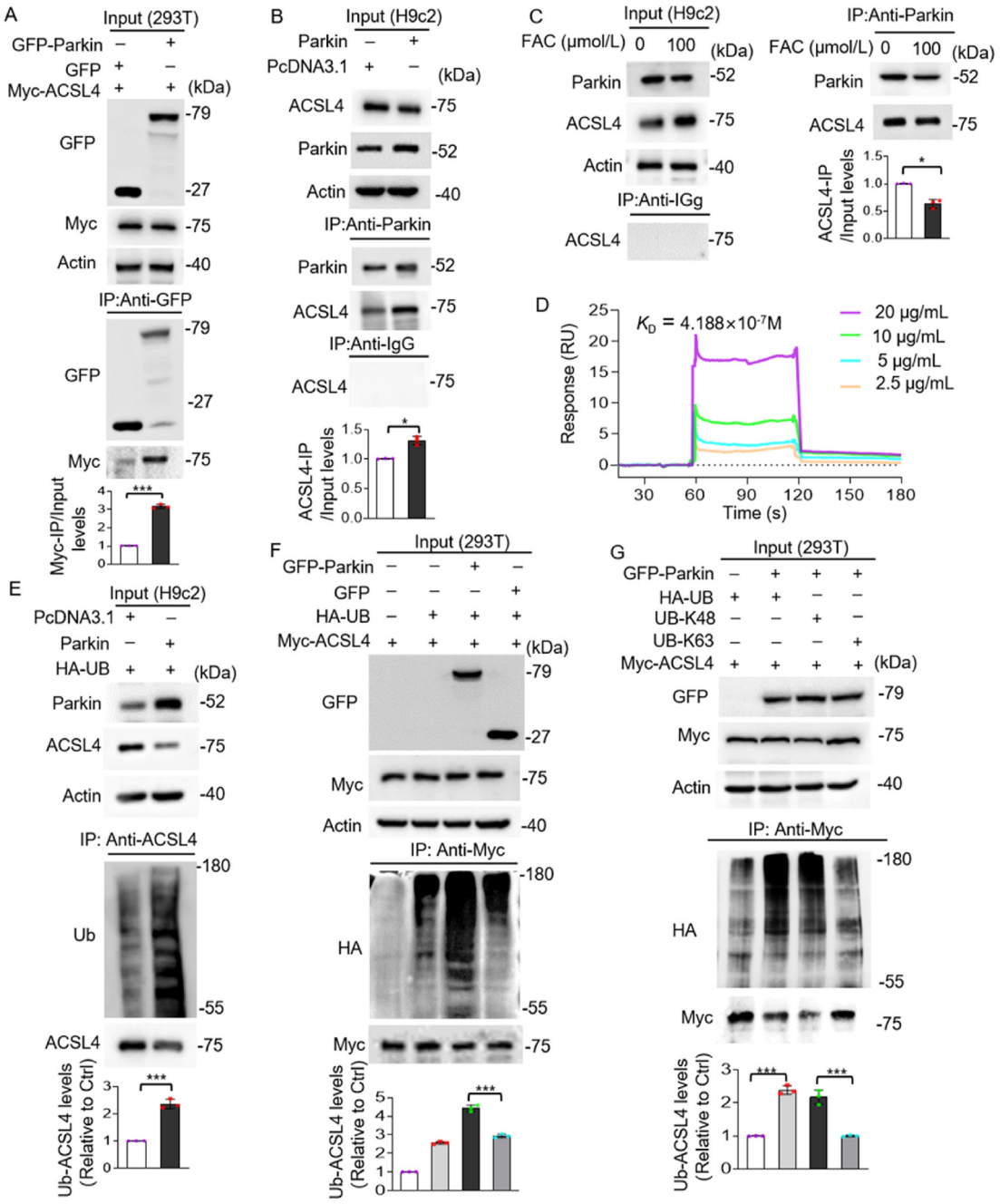

Figure 5 Parkin binds ACSL4 and catalyzes the ubiquitination of ACSL4. (A–C) Immunoprecipitation (IP) was used to detect the interaction between Parkin and ACSL4. (A) HEK 293T cells were transfected with Myc-ACSL4 along with GFP-Parkin or GFP plasmids, Myc-ACSL4 was immunoprecipitated with GFP and GFP-Parkin in HEK293T cells. (B) Cardiomyocytes H9c2 were transfected Parkin overexpressing plasmid or control PcDNA3.1, Parkin was immunoprecipitated with ACSL4 and Parkin in cardiomyocytes. (C) Cardiomyocytes were treated with 100 μmol/L FAC for 6 h, and the endogenous interaction between Parkin and ACSL4 was evaluated by IP. (D) Surface plasmon resonance (SPR) sensorgrams of the binding of an increasing amount of ACSL4 to Parkin ligand captured on a CM5 chip. (E–G) Parkin ubiquitination modified ACSL4. (E) Cardiomyocytes were transfected with HA-ubiquitin along with Parkin overexpression plasmid or control PcDNA3.1, respectively. Ubiquitination of ACSL4 was analyzed by IP in cardiomyocytes. (F) HEK293T cells were transfected with Myc-ACSL4 along with HA-ubiquitin and GFP-Parkin or GFP plasmids. The ubiquitination level of ACSL4 was analyzed by IP. (G) Parkin catalyzed polyubiquitination of the K48 linkage of ACSL4. HEK293T cells were transfected with Myc-ACSL4 along with HA-ubiquitin and GFP-Parkin or K48 ubiquitin or K63 ubiquitin. Ubiquitination of ACSL4 was analyzed by IP. $n = 3$ experiments per group.

Moreover, mice fed a high-iron diet presented increased cardiac fibrosis, as evidenced by elevated levels of Masson, SMA, and CTGF proteins (Fig. 7H and I, Fig. S7C). Notably, these effects were aggravated in *Myh6-CreER^{T2}/Parkin$^{fl/fl}$* mice (Fig. 7H and I, Fig. S7C). We also assessed the extent of myocardial injury caused by iron overload by measuring

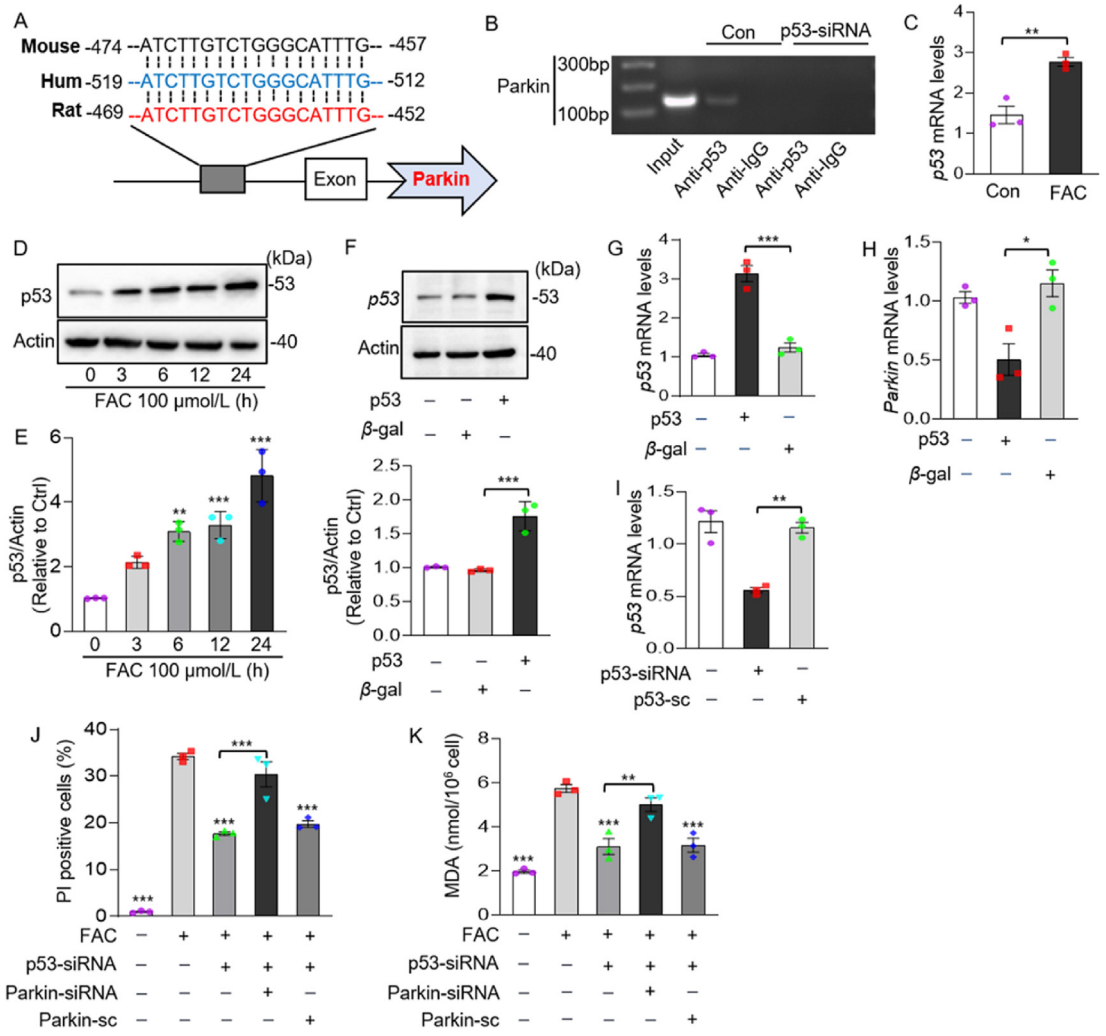

Figure 6 p53 targets Parkin regulating iron overload-induced ferroptosis. (A, B) p53 binds to and transactivates the p53 responsive element in rat *Parkin* gene. (A) The putative binding site in mouse, human and rat *Parkin* gene predicted by the transcription factor website. Numbers indicate the nucleotide position relative to the ATG site. (B) ChIP analysis of interactions between p53 in rat *Parkin* gene in cardiomyocytes. Cardiomyocytes were transfected with p53-siRNA for 24 h, cells were harvested for the ChIP analysis. Chromatin-bound DNA was immunoprecipitated with the anti-p53 antibody. Anti-igG antibody was used as a negative control. (C−E) Cardiomyocytes H9c2 were treated with 100 μmol/L FAC for 24 h, p53 mRNA (C) and protein (D, E) levels were detected by RT-PCR and immunoblot. (E) The quantitative analysis of immunoblot. (F−H) p53 protein levels (F), quantification is shown on the right, p53 mRNA (G), and Parkin mRNA levels (H) were detected by immunoblot and RT-PCR after transfection of p53 overexpression virus and control β-gal 24 h. (F) *p53* mRNA levels were detected after transfection of p53-siRNA and control p53-sc 24 h. (I−K) Knockdown of p53 by its siRNA inhibits iron overload-induced cell death (J) and lipid peroxidation (K) in cardiomyocytes exposed to 100 μmol/L FAC, which was attenuated by knockdown of Parkin. Data are expressed as mean ± SD, $*P < 0.05$; $**P < 0.01$; $***P < 0.001$ significant, one-way ANOVA. $n = 3$.

lactate dehydrogenase (LDH) release, creatine kinase isoenzyme (CK-MB) and cardiac troponin T (cTnT) levels. The results reveal increased LDH release (Fig. S7D), elevated CK-MB and cTnT content (Fig. S7E and S7F), and increased heart-to-body weight in the high-iron diet-fed mice (Fig. S7G); these effects were also aggravated in the *Myh6-CreER^{T2}/Parkin$^{fl/fl}$* mice (Fig. S7D−S7G). Additionally, we evaluated cardiac function *via* ultrasound, which revealed a reduced ejection fraction (EF) (Fig. S7H) and fractional shortening of the left ventricular diameter (FS) (Fig. S7I), as well as increased systolic left ventricular internal diameters (LVIDs) (Fig. S7J), suggesting impaired cardiac function due to the high-iron diet. These findings further support the idea that the high-iron diet caused myocardial injury in mice and may be associated with ferroptosis, *Myh6-CreER^{T2}/Parkin$^{fl/fl}$* mice also exhibited aggravated iron overload-induced myocardial injury (Fig. S7D−S7G). Additionally, we also investigated whether mitophagy is involved in iron overload-induced myocardial injury *in vivo*. The expression levels of mitophagy-associated proteins were reduced in hearts of high-iron diet mice, which was consistent with the results at the cellular level (Fig. S7K and S7L).

We subsequently hypothesized that the reintroduction of Parkin in cardiac-specific Parkin knockout cardiomyocytes would restore ACSL4 ubiquitination promotion and ferroptosis. We generated cardiac-specific Parkin knockout primary cardiomyocytes and then transfected them with Parkin overexpression plasmid to evaluate the impact of their effects on ACSL4 ubiquitination and ferroptosis. The results reveal that the

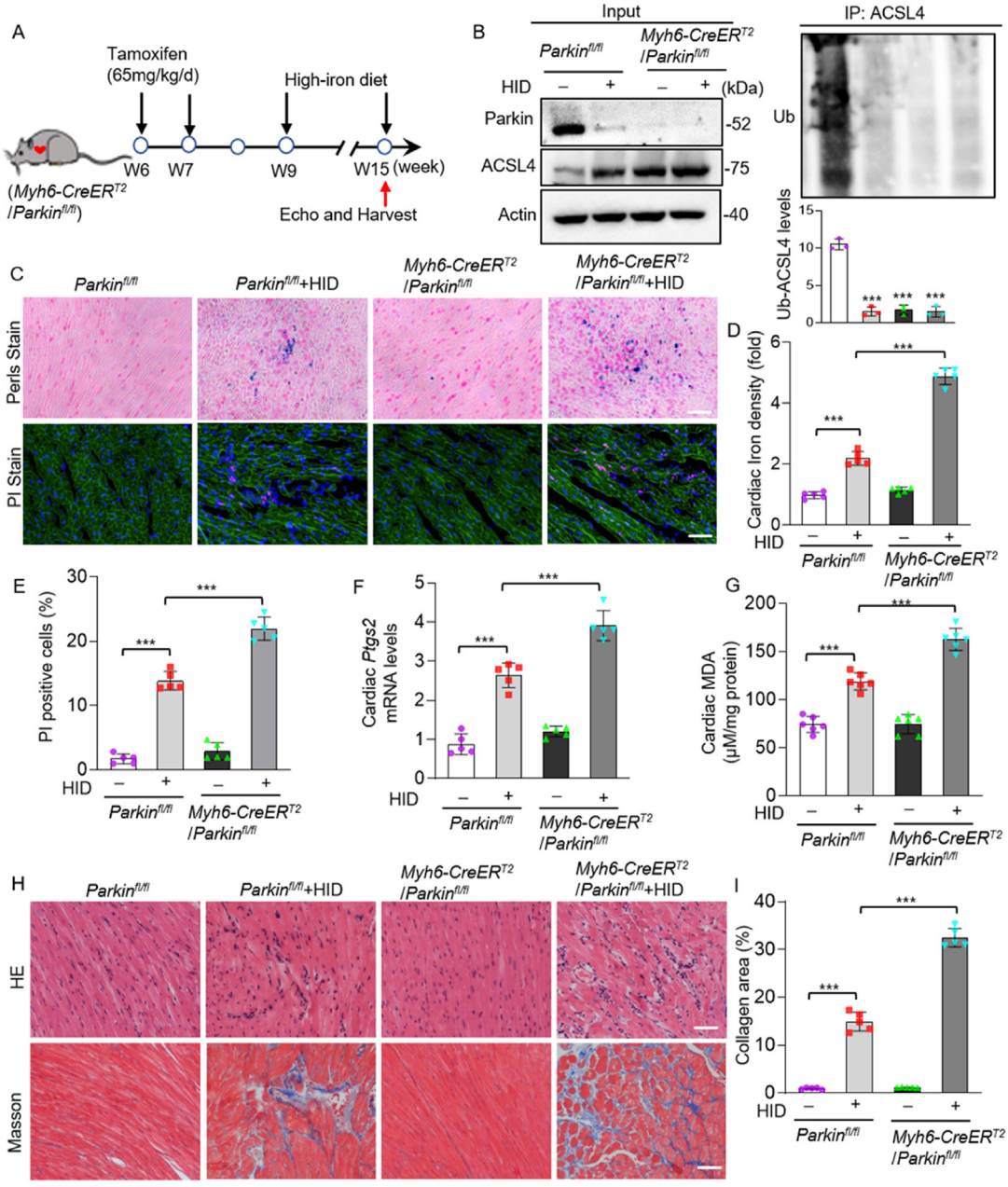

Figure 7 Iron-overloaded *Myh6-CreER*^{T2}*/Parkin*$^{fl/fl}$ mice exhibit elevated levels of tissue ferroptosis and myocardial injury. (A) Schematic diagram showing the mouse model of *Myh6-CreER*^{T2}*/Parkin*$^{fl/fl}$ high-iron diet. (A−I) *Parkin*$^{fl/fl}$ and *Myh6-CreER*^{T2}*/Parkin*$^{fl/fl}$ mice were fed a high iron diet for 6 weeks, and control mice were fed a normal diet, (B) Immunoblot was performed to detect Parkin, ACSL4 protein levels, immunoprecipitation (IP) was used to detect the Parkin ubiquitination modified ACSL4, quantification is shown in the lower panel. (C) Perls staining to measure iron levels (Top), iron-positive are shown in blue, (D) quantification is shown on the right. Scale bar: 100 μm. (C, E) PI staining to measure cell death (Bottom). PI was injected into the mice to label positive cells 1 h before the execution. (C) Representative image of myocardial tissue section, (E) the quantitative analysis of PI-positive cells. PI-positive myocyte nuclei (red), 4′,6-diaminyl-2-phenylindole stained nuclei (blue), cardiomyocytes were labeled by α-actinin (green). Scale bar: 100 μm. (F) The *Ptgs2* mRNA levels were detected by RT-PCR and (G) lipid peroxidation was detected by MDA reagent assay. (H) Cardiac tissue sections were prepared from the mice and stained with HE (Top) or Masson's trichrome staining (Bottom). Representative photomicrographs show collagen areas by Masson's trichrome staining (H). Collagen area was quantitatively analyzed (I). Scale bar: 100 μm. Data are expressed as mean ± SD, $*P < 0.05$; $**P < 0.01$; $***P < 0.001$ significant, one-way ANOVA. $n = 5$.

re-expression of Parkin in cardiac-specific Parkin knockout primary cardiomyocytes promoted ACSL4 ubiquitination and inhibited ferroptosis (Supporting Information Fig. S8A and S8B).

3.9. *Fer-1 and Parkin attenuate I/R-induced myocardial injury*

To further investigate the role of ferroptosis in cardiac I/R injury and the relationship between iron overload and I/R injury, we

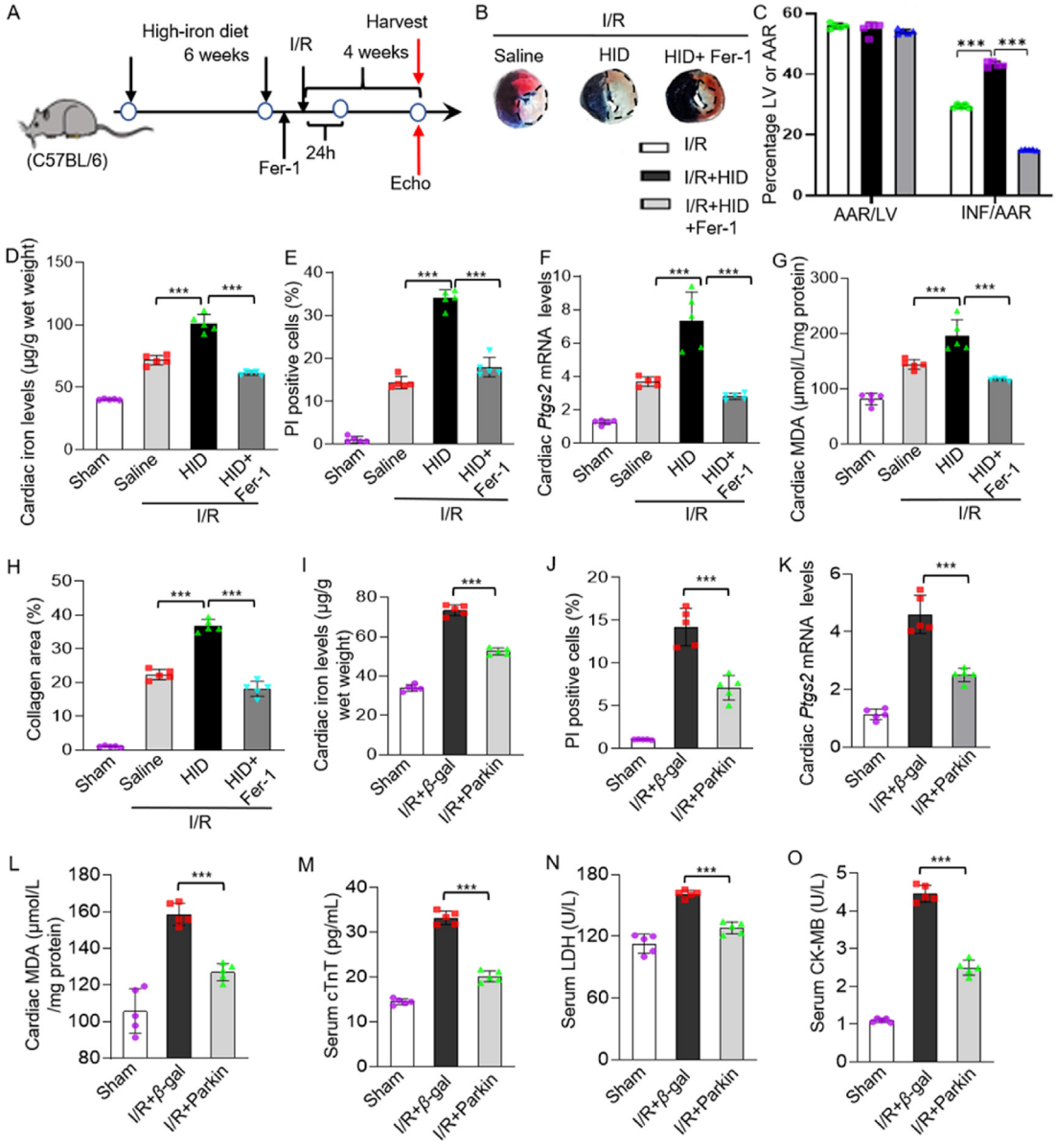

Figure 8 Fer-1 and Parkin attenuates I/R-induced myocardial injury. (A) Schematic diagram showing the mouse model of I/R injury. Representative images (B) and quantitative data (C) for infarct size (INF) and relative area at risk (AAR) in heart sections obtained from mice subjected to 30 min/24 h I/R injury and treated with saline (control) or Fer-1. Red, Danger Zone (AAR); White, infarct area (INF); Blue, non-hazardous area. (D) Cardiac iron levels, (E) cell death, (F) *Ptgs2* mRNA levels, (G) MDA levels measured in mice subjected to sham surgery or 30 min/24 h I/R injury and treated with saline and Fer-1. (H) Masson's trichrome staining of heart sections obtained from mice subjected to sham surgery or 30 min/4 weeks I/R injury and treated with saline and Fer-1. (I−M) Mice were injected with Parkin overexpressing adenovirus or control *β*-gal *via* intravenous injection into the tail, after 3 weeks, the mice were subjected to sham or I/R surgery. Blood and heart samples were collected for measure (I) cardiac iron levels, (J) cell death, (K) *Ptgs2* mRNA levels, (L) MDA levels, (M) cTnT levels, (N) LDH levels and (O) CK-MB levels. Data are expressed as mean ± SD, $^{*}P < 0.05$; $^{**}P < 0.01$; $^{***}P < 0.001$ significant, one-way ANOVA. $n = 5$.

conducted experiments with C57BL/6 mice. The mice were fed a high-iron diet for 6 weeks and subjected to I/R surgery. Additionally, the mice were injected with Fer-1 one day before I/R surgery (Fig. 8A). We observed an increase in MI size in the mice fed a high-iron diet compared with those fed a standard diet (Fig. 8B and C). The infarction size decreased after the Fer-1 injection (Fig. 8B and C). Furthermore, compared with the sham operation group, the I/R-treated group showed increased myocardial iron content (Fig. 8D), percentage of myocardial cell death (Fig. 8E and Supporting Information Fig. S9A), and *Ptgs2* mRNA (Fig. 8F), and MDA (Fig. 8G) levels. However, the injection of Fer-1 into mice reduced ferroptosis during cardiac I/R injury, leading to a decrease in these parameters (Fig. 8D−G).

Iron overload exacerbated I/R-induced myocardial remodeling and cardiac injury (Fig. 8H and Fig. S9B−S9D), but these effects were inhibited by Fer-1 injection. Additionally, the high-iron diet led to an increase in the heart-to-body weight ratio (Fig. S9E), and worsened cardiac function impairment (Fig. S9F−S9H) in I/R-treated mice. However, these effects were also suppressed after Fer-1 treatment (Fig. S9F−S9H). These findings suggest that iron

overload exacerbated myocardial ferroptosis induced by I/R and impaired cardiac function and that Fer-1 attenuated iron overload-induced myocardial injury.

We wanted to know whether Parkin overexpression in the heart can ameliorate myocardial injury. Thus, we constructed a Parkin overexpression model to investigate the effects of Parkin on I/R-induced ferroptosis and myocardial injury. Our previous work revealed that Parkin overexpression inhibits I/R-induced infarct size, myocardial remodeling, and impaired cardiac function[48]. Furthermore, we observed that the overexpression of Parkin effectively suppressed the ferroptosis and myocardial damage induced by I/R (Fig. 8I−O). These results suggest that Fer-1 and Parkin overexpression ameliorated I/R-induced ferroptosis and myocardial injury *in vivo*.

4. Discussion

Currently, the causes of iron overload in clinical settings include primary iron overload and secondary iron overload[49]. Primary iron overload is an autosomal recessive genetic disorder caused by gene mutations that encode various iron transport and iron-sensing proteins in hereditary hemochromatosis. Secondary iron overload is induced mainly by repeated blood transfusions, drug toxicity, or improper dietary outcomes. Iron overload increases the risk of cardiovascular diseases such as hereditary hypopigmentation, cardiac I/R injury, and myocardial infarction[7,11]. Oxidative stress is the primary factor responsible for myocardial injury caused by iron overload[50]. In heart tissue, oxidative stress impairs excitation−contraction coupling, damages cell membranes and mitochondrial membranes through lipid peroxidation, inhibits mitochondrial oxidative phosphorylation and ATP levels, and causes DNA and mitochondrial DNA (mtDNA) damage[51].Ferroptosis, a form of cell death, depends on iron, and iron overload induces ferroptosis in cardiomyocytes, increases mitochondrial iron levels, and disrupts mitochondrial function[52,53]. Iron reportedly promotes lipid peroxidation through the Haber−Weiss and Fenton reactions[51]. However, our findings indicate that iron-regulated lipid metabolism through the p53−Parkin−ACSL4 pathway, suggesting that the mechanism of iron involvement in ferroptosis is regulated by multiple proteins rather than solely by chemical reactions. Additionally, our results demonstrate that iron overload worsened myocardial infarction and that inhibiting iron or ferroptosis alleviated myocardial injury, which may provide a promising direction for the study of cardiovascular disease.

Parkin is highly expressed in the heart and plays a critical cardioprotective role in cardiovascular diseases, including cardiac development, myocardial infarction, myocardial I/R injury, and cardiotoxicity[31,40,48]. Parkin directs cardiac metabolic maturation and mitochondria removal during the perinatal period[32]. Cardiomyocyte-specific ablation of *Park2*, encodes Parkin, which inhibits mitochondrial maturation after birth and fails to act on MFN2 to regulate mitophagy, resulting in rapid lethality in most mice. In response to I/R injury, *Parkin* transgenic mice exhibit improved cardiac remodeling and function *via* suppression of the mPTP opening by catalyzing the ubiquitination of CypD in necrotic cascades[48]. In addition, Parkin transgenic mice attenuate DOX-induced cardiotoxicity by promoting mitophagy and inhibiting apoptosis[40]. Intriguingly, we have initially demonstrated that Parkin inhibits iron overload and ischemia-induced myocardial injury by preventing ferroptosis. Additionally, our animal studies have indicated that overexpression of Parkin mitigates I/R-induced myocardial injury. However, a limitation of our work is the utilization of the Parkin adenovirus for overexpression instead of a heart-specific Parkin overexpression system. Therefore, future verification should involve the use of heart-specific Parkin knock-in mice or Adeno-associated virus (AAV) delivery system. Notably, iron overload-induced cardiac-specific *Parkin* knockout mice exhibit increased levels of tissue ferroptosis. Thus, our results suggest that the Parkin protein may serve as a novel therapeutic target for cardiomyopathy.

Our findings indicate that iron overload led to a decrease in mitophagy, but the overexpression of Parkin promoted mitophagy to inhibit ferroptosis. These results suggest a potential relationship between mitophagy and ferroptosis. Previous studies have also suggested a connection between mitophagy and ferroptosis. For example, ferritinophagy facilitates the release of free iron and renders cells more susceptible to ferroptosis[54]. Ferroptosis drives vascular aging by inducing NAD^+ loss and promoting NCOA4-mediated ferritinophagy[55]. Mitophagy leads to lysosomal degradation of lipid droplet mitochondria, release of free fatty acids, and a significant increase in lipid peroxidation, thus promoting Ferroptosis[56]. In contrast, mitophagy may lead to the sequestration of iron into mitophagosomes, thereby reducing the source of reactive oxygen species (ROS) required for ferroptosis[57]. The relationship between mitophagy and ferroptosis is complex, and the potential role of Parkin in mediating ferritinophagy warrants further investigation in the future.

ACSL4 is a critical protein in the regulatory network of ferroptosis-related lipid metabolism. ACSL4 is a long-chain acyl-CoA synthetase (ACS) family protein that is localized primarily in the peroxisome and mitochondria-associated endoplasmic reticulum[58]. ACSL4 activates the conversion of long-chain PUFAs into fatty acyl-CoA to participate in the synthesis of phospholipids in membranes, where long-chain PUFAs are readily oxidized to trigger ferroptosis[59]. ACSL4 was recently found to facilitate the esterification of arachidonic acid (AA) in PE, a process closely related to ferroptosis[45]. The inhibition of PUFA levels by genetic and pharmacological inhibition of ACSL4 triggers the antiferroptosis pathway[45]. Recent research has indicated that ACSL4-mediated lipid metabolism is linked to the occurrence and progression of tumors, such as hepatocellular carcinoma, glioma, and gastric cancer[60-62]. Moreover, inhibiting ACSL4-mediated lipid metabolism could alleviate tissue damage resulting from intestinal I/R[62]. In addition, the substrate of ACSL4, arachidonic acid, causes the release of cytochrome *c*, defects in myocardial cells, and lipid peroxidation in myocardial cells. This process induces ferroptosis, which promotes cardiac remodeling caused by a high-fat diet[63]. However, the suppression of ACSL4 downregulates these effects. Therefore, these findings imply that ACSL4-mediated PUFA−lipid metabolism plays a crucial regulatory role in numerous diseases. In contrast, monounsaturated fatty acids (MUFAs) have been reported to inhibit lipid peroxidation and maintain cellular membrane integrity in organisms, which play a crucial role in longevity[64]. Thus, further exploration of whether MUFAs exert a protective effect on cardiac injury induced by iron overload is worthwhile.

Several enzymes are involved in the synthesis of fatty acids on phospholipid backbones. One example is lysophosphatidylcholine acyltransferase 3, which ubiquitinates PUFAs into membrane phospholipids. Therefore, deleting this enzyme increases cellular resistance to ferroptosis[65]. Lipoxygenase is an iron-containing enzyme that can directly oxidize PUFAs and lipids containing PUFAs in cell membranes. It plays a crucial role in the metabolism of unsaturated fatty acids, converting arachidonic acid, linoleic acid, and other unsaturated fatty acids into bioactive metabolites[66]. Additionally, phosphatidyl ethanolamine binding protein 1, a scaffold protein that

inhibits protein kinase cascades, has been found to bind to the lipid oxygenase ALOX15 in the membrane. This binding redirects the enzyme toward PUFAs, thereby promoting ferroptosis[67]. Consequently, changes in the levels of PUFAs in phospholipids are likely crucial factors in the development of ferroptosis. Our study revealed an increase in the levels of PUFAs such as eicosapentaenoic acid, docosahexaenoic acid, and docosahexaenoic acid. However, inhibiting ACSL4 prevented the increase in polyunsaturated fatty acid levels and the occurrence of ferroptosis. These findings indicate that the peroxidation of PUFA phospholipids contributes to the regulation of myocardial injury; however, further research is needed to determine the underlying mechanism involved.

By regulating apoptosis or necrosis, p53 is closely associated with MI and other cardiovascular diseases[68,69]. Our results suggest that p53 may also be involved in myocardial damage through the regulation of ferroptosis. It has been reported that p53 has an essential regulatory role in ferroptosis. However, the results are controversial. As a well-known transcription factor, p53 has powerful functions in the transcription of numerous genes. Studies have shown that p53 can promote ferroptosis in tumor cells through the transcriptional inhibition of *SLC711A* to synthesize glutathione[70]. p53 indirectly activates ALOX12 by transcriptionally inhibiting *SLC7A11*, which ultimately leads to ALOX12-dependent ferroptosis[71]. Other studies have shown that p53 can inhibit ferroptosis in colorectal cancer or human fibrosarcoma cells by inhibiting dipeptidyl peptidase-4 (DPP4, a lipid metabolism regulator) activity[72]. In our research, we observed that p53 promoted ferroptosis by transcriptionally repressing Parkin expression. In addition, p53 was regulated by iron levels. Moreover, p53 expression was found to increase in myocardial I/R injury models, leading to the transcriptional activation of *TfR1*, an iron transporter that is involved in the uptake of iron from the blood to heart cells, thus inducing myocardial injury[73]. Our research demonstrated that FAC treatment resulted in elevated levels of p53 in cardiomyocytes, and subsequently, p53 triggered cardiomyocyte ferroptosis. This finding is consistent with that of a previous study, which suggested that p53 may form a positive feedback pathway in the regulation of iron, which exacerbates myocardial injury. Furthermore, the investigation of negative regulators is particularly intriguing in the context of modulating the p53 response, as these factors may represent potential targets for activating p53 function. iPLA2β-mediated lipid detoxification is critically involved in suppressing p53-mediated ferroptosis in cancers[74]. However, whether this mechanism plays an important role in iron-overload induced cardiomyopathy needs further study.

5. Conclusions

In summary, our findings suggest that iron overload resulted in Parkin depletion and that Parkin overexpression rescued ferroptosis through the ubiquitination of ACSL4. In addition, iron overload-induced Parkin depletion might be mediated by increased p53 expression. Thus, our study identified a novel antiferroptosis pathway involving p53−Parkin−ACSL4, providing new insights into the regulatory network of ferroptosis. Although research on iron and ferroptosis in cardiac diseases is still in its early stages and the regulatory network is not fully understood, identifying new target proteins and regulatory mechanisms to inhibit iron overload and ferroptosis represents a promising direction for the prevention and treatment of cardiac diseases.

Acknowledgments

This work was supported by the National Natural Science Foundation of China (Grant No. 82270301); The Natural Science Foundation of Shandong Province (Grant No. ZR2019ZD28, China); and the Taishan Scholar Program of Shandong Province (Grant No. 19-6-1-6-nsh, China).

Author contributions

Dandan Xiao: Writing − original draft, Validation, Software, Investigation, Formal analysis, Data curation. Wenguang Chang: Writing − review & editing, Formal analysis, Data curation. Xiang Ao: Supervision, Software, Investigation. Lin Ye: Formal analysis, Data curation, Conceptualization. Weiwei Wu: Writing − original draft, Methodology. Lin Song: Software, Methodology, Investigation. Xiaosu Yuan: Investigation, Formal analysis. Luxin Feng: Resources, Investigation. Peiyan Wang: Validation, Software, Resources. Yu Wang: Methodology, Investigation, Formal analysis. Yi Jia: Software, Investigation, Formal analysis. Xiaopeng Tang: Methodology, Formal analysis, Data curation. Jianxun Wang: Writing − review & editing, Validation, Resources, Project administration, Funding acquisition, Formal analysis, Data curation, Conceptualization.

Conflicts of interest

The authors declare no conflict of interest.

Appendix A. Supporting information

Supporting information to this article can be found online at https://doi.org/10.1016/j.apsb.2024.12.027.

References

1. Zhang C. Essential functions of iron-requiring proteins in DNA replication, repair and cell cycle control. *Protein Cell* 2014;**5**:750−60.
2. Fernández Real JM, López Bermejo A, Ricart W. Cross-talk between iron metabolism and diabetes. *Diabetes* 2002;**51**:2348−54.
3. Morales M, Xue X. Targeting iron metabolism in cancer therapy. *Theranostics* 2021;**11**:8412−29.
4. Zhang J, Song Y, Li Y, Lin HB, Fang X. Iron homeostasis in the heart: molecular mechanisms and pharmacological implications. *J Mol Cell Cardiol* 2023;**174**:15−24.
5. Ito J, Omiya S, Rusu MC, Ueda H, Murakawa T, Tanada Y, et al. Iron derived from autophagy-mediated ferritin degradation induces cardiomyocyte death and heart failure in mice. *Elife* 2021;**10**:e62174.
6. Koleini N, Shapiro JS, Geier J, Ardehali H. Ironing out mechanisms of iron homeostasis and disorders of iron deficiency. *J Clin Invest* 2021;**131**:e148671.
7. Miyamoto HD, Ikeda M, Ide T, Tadokoro T, Furusawa S, Abe K, et al. Iron overload *via* heme degradation in the endoplasmic reticulum triggers ferroptosis in myocardial ischemia-reperfusion injury. *JACC Basic Transl Sci* 2022;**7**:800−19.
8. Bulluck H, Rosmini S, Abdel Gadir A, White SK, Bhuva AN, Treibel TA, et al. Residual myocardial iron following intramyocardial hemorrhage during the convalescent phase of reperfused ST-segment-elevation myocardial infarction and adverse left ventricular remodeling. *Circ Cardiovasc Imaging* 2016;**9**:e004940.
9. Anker SD, Comin Colet J, Filippatos G, Willenheimer R, Dickstein K, Drexler H, et al. Ferric carboxymaltose in patients with heart failure and iron deficiency. *N Engl J Med* 2009;**361**:2436−48.

10. Fang X, Wang H, Han D, Xie E, Yang X, Wei J, et al. Ferroptosis as a target for protection against cardiomyopathy. *Proc Natl Acad Sci U S A* 2019;**116**:2672−80.
11. Tang WH, Wu S, Wong TM, Chung SK, Chung SSM. Polyol pathway mediates iron-induced oxidative injury in ischemic−reperfused rat heart. *Free Radic Biol Med* 2008;**45**:602−10.
12. Tuo QZ, Lei P, Jackman KA, Li XL, Xiong H, Li XL, et al. Tau-mediated iron export prevents ferroptotic damage after ischemic stroke. *Mol Psychiatry* 2017;**22**:1520−30.
13. Ichikawa Y, Ghanefar M, Bayeva M, Wu R, Khechaduri A, Naga Prasad SV, et al. Cardiotoxicity of doxorubicin is mediated through mitochondrial iron accumulation. *J Clin Invest* 2014;**124**:617−30.
14. Dixon SJ, Lemberg KM, Lamprecht MR, Skouta R, Zaitsev EM, Gleason CE, et al. Ferroptosis: an iron-dependent form of non-apoptotic cell death. *Cell* 2012;**149**:1060−72.
15. Jiang X, Stockwell BR, Conrad M. Ferroptosis: mechanisms, biology and role in disease. *Nat Rev Mol Cell Biol* 2021;**22**:266−82.
16. Kagan VE, Mao G, Qu F, Angeli JPF, Doll S, Croix CS, et al. Oxidized arachidonic and adrenic PEs navigate cells to ferroptosis. *Nat Chem Biol* 2017;**13**:81−90.
17. Fu J, Zhang P, Sun Z, Lu G, Cao Q, Chen Y, et al. A combined nanotherapeutic approach targeting farnesoid X receptor, ferroptosis, and fibrosis for nonalcoholic steatohepatitis treatment. *Acta Pharm Sin B* 2024;**14**:2228−46.
18. Wang X, Chen X, Zhou W, Men H, Bao T, Sun Y, et al. Ferroptosis is essential for diabetic cardiomyopathy and is prevented by sulforaphane *via* AMPK/NRF2 pathways. *Acta Pharm Sin B* 2022;**12**:708−22.
19. Zhang X, Zheng C, Gao Z, Chen H, Li K, Wang L, et al. SLC7A11/xCT prevents cardiac hypertrophy by inhibiting ferroptosis. *Cardiovasc Drugs Ther* 2022;**36**:437−47.
20. Yang X, Kawasaki NK, Min J, Matsui T, Wang F. Ferroptosis in heart failure. *J Mol Cell Cardiol* 2022;**173**:141−53.
21. Yu W, Hu Y, Liu Z, Guo K, Ma D, Peng M, et al. Sorting nexin 3 exacerbates doxorubicin-induced cardiomyopathy *via* regulation of TFRC-dependent ferroptosis. *Acta Pharm Sin B* 2023;**13**:4875−92.
22. Qiu H, Huang S, Liu Y, Liu L, Guo F, Guo Y, et al. Idebenone alleviates doxorubicin-induced cardiotoxicity by stabilizing FSP1 to inhibit ferroptosis. *Acta Pharm Sin B* 2024;**14**:2581−97.
23. Dabkowski ER, Williamson CL, Hollander JM. Mitochondria-specific transgenic overexpression of phospholipid hydroperoxide glutathione peroxidase (GPx4) attenuates ischemia/reperfusion-associated cardiac dysfunction. *Free Radic Biol Med* 2008;**45**:855−65.
24. Gao M, Monian P, Quadri N, Ramasamy R, Jiang X. Glutaminolysis and transferrin regulate ferroptosis. *Mol Cell* 2015;**59**:298−308.
25. Tong J, Li D, Meng H, Sun D, Lan X, Ni M, et al. Targeting a novel inducible GPX4 alternative isoform to alleviate ferroptosis and treat metabolic-associated fatty liver disease. *Acta Pharm Sin B* 2022;**12**:3650−66.
26. Kitada T, Asakawa S, Hattori N, Matsumine H, Yamamura Y, Minoshima S, et al. Mutations in the parkin gene cause autosomal recessive juvenile parkinsonism. *Nature* 1998;**392**:605−8.
27. Hwang CJ, Kim YE, Son DJ, Park MH, Choi DY, Park PH, et al. Parkin deficiency exacerbate ethanol-induced dopaminergic neurodegeneration by P38 pathway dependent inhibition of autophagy and mitochondrial function. *Redox Biol* 2017;**11**:456−68.
28. Lutz AK, Exner N, Fett ME, Schlehe JS, Kloos K, Lämmermann K, et al. Loss of parkin or PINK1 function increases Drp1-dependent mitochondrial fragmentation. *J Biol Chem* 2009;**284**:22938−51.
29. Vives Bauza C, Zhou C, Huang Y, Cui M, de Vries RLA, Kim J, et al. PINK1-dependent recruitment of Parkin to mitochondria in mitophagy. *Proc Natl Acad Sci U S A* 2010;**107**:378−83.
30. Pickrell AM, Youle RJ. The roles of PINK1, parkin, and mitochondrial fidelity in Parkinson's disease. *Neuron* 2015;**85**:257−73.
31. Dorn GW. Parkin-dependent mitophagy in the heart. *J Mol Cell Cardiol* 2016;**95**:42−9.
32. Gong G, Song M, Csordas G, Kelly DP, Matkovich SJ, Dorn GW. Parkin-mediated mitophagy directs perinatal cardiac metabolic maturation in mice. *Science* 2015;**350**:aad2459.
33. Kubli DA, Zhang X, Lee Y, Hanna RA, Quinsay MN, Nguyen CK, et al. Parkin protein deficiency exacerbates cardiac injury and reduces survival following myocardial infarction. *J Biol Chem* 2013;**288**:915−26.
34. Wang S, Zhao Z, Feng X, Cheng Z, Xiong Z, Wang T, et al. Melatonin activates Parkin translocation and rescues the impaired mitophagy activity of diabetic cardiomyopathy through Mst1 inhibition. *J Cell Mol Med* 2018;**22**:5132−44.
35. Woodall BP, Orogo AM, Najor RH, Cortez MQ, Moreno ER, Wang H, et al. Parkin does not prevent accelerated cardiac aging in mitochondrial DNA mutator mice. *JCI Insight* 2019;**5**:e127713.
36. Das SK, Patel VB, Basu R, Wang W, DesAulniers J, Kassiri Z, et al. Females are protected from iron-overload cardiomyopathy independent of iron metabolism: key role of oxidative stress. *J Am Heart Assoc* 2017;**6**:e003456.
37. Fang X, Cai Z, Wang H, Han D, Cheng Q, Zhang P, et al. Loss of cardiac ferritin H facilitates cardiomyopathy *via* Slc7a11-mediated ferroptosis. *Circ Res* 2020;**127**:486−501.
38. Wang K, Long B, Liu F, Wang JX, Liu CY, Zhao B, et al. A circular RNA protects the heart from pathological hypertrophy and heart failure by targeting miR-223. *Eur Heart J* 2016;**37**:2602−11.
39. Wang JX, Zhang XJ, Li Q, Wang K, Wang Y, Jiao JQ, et al. MicroRNA-103/107 regulate programmed necrosis and myocardial ischemia/reperfusion injury through targeting FADD. *Circ Res* 2015;**117**:352−63.
40. Xiao D, Chang W, Ding W, Wang Y, Fa H, Wang J. Enhanced mitophagy mediated by the YAP/Parkin pathway protects against DOX-induced cardiotoxicity. *Toxicol Lett* 2020;**330**:96−107.
41. Yang WS, SriRamaratnam R, Welsch ME, Shimada K, Skouta R, Viswanathan VS, et al. Regulation of ferroptotic cancer cell death by GPX4. *Cell* 2014;**156**:317−31.
42. Fleming RE, Ponka P. Iron overload in human disease. *N Engl J Med* 2012;**366**:348−59.
43. Conrad M, Proneth B. Broken hearts: iron overload, ferroptosis and cardiomyopathy. *Cell Res* 2019;**29**:263−4.
44. Martín Maestro P, Gargini R, Perry G, Avila J, García Escudero V. PARK2 enhancement is able to compensate mitophagy alterations found in sporadic Alzheimer's disease. *Hum Mol Genet* 2016;**25**:792−806.
45. Doll S, Proneth B, Tyurina YY, Panzilius E, Kobayashi S, Ingold I, et al. ACSL4 dictates ferroptosis sensitivity by shaping cellular lipid composition. *Nat Chem Biol* 2017;**13**:91−8.
46. Husnjak K, Dikic I. Ubiquitin-binding proteins: decoders of ubiquitin-mediated cellular functions. *Annu Rev Biochem* 2012;**81**:291−322.
47. Zhang C, Lin M, Wu R, Wang X, Yang B, Levine AJ, et al. Parkin, a p53 target gene, mediates the role of p53 in glucose metabolism and the Warburg effect. *Proc Natl Acad Sci U S A* 2011;**108**:16259−64.
48. Sun T, Ding W, Xu T, Ao X, Yu T, Li M, et al. Parkin regulates programmed necrosis and myocardial ischemia/reperfusion injury by targeting cyclophilin-D. *Antioxid Redox Signal* 2019;**31**:1177−93.
49. Das SK, Wang W, Zhabyeyev P, Basu R, McLean B, Fan D, et al. Iron-overload injury and cardiomyopathy in acquired and genetic models is attenuated by resveratrol therapy. *Sci Rep* 2015;**5**:18132.
50. Berdoukas V, Coates TD, Cabantchik ZI. Iron and oxidative stress in cardiomyopathy in thalassemia. *Free Radic Biol Med* 2015;**88**:3−9.
51. Schiattarella GG, Hill JA. Metabolic control and oxidative stress in pathological cardiac remodelling. *Eur Heart J* 2017;**38**:1399−401.
52. Fefelova N, Wongjaikam S, Pamarthi SH, Siri Angkul N, Comollo T, Kumari A, et al. Deficiency of mitochondrial calcium uniporter abrogates iron overload-induced cardiac dysfunction by reducing ferroptosis. *Basic Res Cardiol* 2023;**118**:21.
53. Ji QX, Zeng FY, Zhou J, Wu WB, Wang XJ, Zhang Z, et al. Ferroptotic stress facilitates smooth muscle cell dedifferentiation in arterial remodelling by disrupting mitochondrial homeostasis. *Cell Death Differ* 2023;**30**:457−74.
54. Yu F, Zhang Q, Liu H, Liu J, Yang S, Luo X, et al. Dynamic *O*-GlcNAcylation coordinates ferritinophagy and mitophagy to activate ferroptosis. *Cell Discov* 2022;**8**:40.

55. Sun DY, Wu WB, Wu JJ, Shi Y, Xu JJ, Ouyang SX, et al. Pro-ferroptotic signaling promotes arterial aging *via* vascular smooth muscle cell senescence. *Nat Commun* 2024;**15**:1429.
56. Yang P, Li J, Zhang T, Ren Y, Zhang Q, Liu R, et al. Ionizing radiation-induced mitophagy promotes ferroptosis by increasing intracellular free fatty acids. *Cell Death Differ* 2023;**30**:2432−45.
57. Yamashita SI, Sugiura Y, Matsuoka Y, Maeda R, Inoue K, Furukawa K, et al. Mitophagy mediated by BNIP3 and NIX protects against ferroptosis by downregulating mitochondrial reactive oxygen species. *Cell Death Differ* 2024;**31**:651−61.
58. Quan J, Bode AM, Luo X. ACSL family: the regulatory mechanisms and therapeutic implications in cancer. *Eur J Pharmacol* 2021;**909**:174397.
59. Yuan H, Li X, Zhang X, Kang R, Tang D. Identification of ACSL4 as a biomarker and contributor of ferroptosis. *Biochem Biophys Res Commun* 2016;**478**:1338−43.
60. Chen J, Ding C, Chen Y, Hu W, Yu C, Peng C, et al. ACSL4 reprograms fatty acid metabolism in hepatocellular carcinoma *via* c-Myc/SREBP1 pathway. *Cancer Lett* 2021;**502**:154−65.
61. Yee PP, Wei Y, Kim SY, Lu T, Chih SY, Lawson C, et al. Neutrophil-induced ferroptosis promotes tumor necrosis in glioblastoma progression. *Nat Commun* 2020;**11**:5424.
62. Li Y, Feng D, Wang Z, Zhao Y, Sun R, Tian D, et al. Ischemia-induced ACSL4 activation contributes to ferroptosis-mediated tissue injury in intestinal ischemia/reperfusion. *Cell Death Differ* 2019;**26**:2284−99.
63. Killion EA, Reeves AR, El Azzouny MA, Yan QW, Surujon D, Griffin JD, et al. A role for long-chain acyl-CoA synthetase-4 (ACSL4) in diet-induced phospholipid remodeling and obesity-associated adipocyte dysfunction. *Mol Metab* 2018;**9**:43−56.
64. Papsdorf K, Miklas JW, Hosseini A, Cabruja M, Morrow CS, Savini M, et al. Lipid droplets and peroxisomes are co-regulated to drive lifespan extension in response to mono-unsaturated fatty acids. *Nat Cell Biol* 2023;**25**:672−84.
65. Cui J, Wang Y, Tian X, Miao Y, Ma L, Zhang C, et al. LPCAT3 is transcriptionally regulated by YAP/ZEB/EP300 and collaborates with ACSL4 and YAP to determine ferroptosis sensitivity. *Antioxid Redox Signal* 2023;**39**:491−511.
66. Mashima R, Okuyama T. The role of lipoxygenases in pathophysiology; new insights and future perspectives. *Redox Biol* 2015;**6**:297−310.
67. Wenzel SE, Tyurina YY, Zhao J, St Croix CM, Dar HH, Mao G, et al. PEBP1 wardens ferroptosis by enabling lipoxygenase generation of lipid death signals. *Cell* 2017;**171**:628−641.e26.
68. Lorenzana Carrillo MA, Gopal K, Byrne NJ, Tejay S, Saleme B, Das SK, et al. TRIM35-mediated degradation of nuclear PKM2 destabilizes GATA4/6 and induces P53 in cardiomyocytes to promote heart failure. *Sci Transl Med* 2022;**14**:eabm3565.
69. Men H, Cai H, Cheng Q, Zhou W, Wang X, Huang S, et al. The regulatory roles of p53 in cardiovascular health and disease. *Cell Mol Life Sci* 2021;**78**:2001−18.
70. Jiang L, Kon N, Li T, Wang SJ, Su T, Hibshoosh H, et al. Ferroptosis as a p53-mediated activity during tumour suppression. *Nature* 2015;**520**:57−62.
71. Chu B, Kon N, Chen D, Li T, Liu T, Jiang L, et al. ALOX12 is required for p53-mediated tumour suppression through a distinct ferroptosis pathway. *Nat Cell Biol* 2019;**21**:579−91.
72. Xie Y, Zhu S, Song X, Sun X, Fan Y, Liu J, et al. The tumor suppressor p53 limits ferroptosis by blocking DPP4 activity. *Cell Rep* 2017;**20**:1692−704.
73. Tang LJ, Zhou YJ, Xiong XM, Li NS, Zhang JJ, Luo XJ, et al. Ubiquitin-specific protease 7 promotes ferroptosis *via* activation of the p53/TfR1 pathway in the rat hearts after ischemia/reperfusion. *Free Radic Biol Med* 2021;**162**:339−52.
74. Chen D, Chu B, Yang X, Liu Z, Jin Y, Kon N, et al. iPLA2β-mediated lipid detoxification controls p53-driven ferroptosis independent of GPX4. *Nat Commun* 2021;**12**:3644.